ACS APPLIED MATERIALS & INTERFACES

www.acsami.org

Research Article

# Enhancement in Site-Specific Delivery of Chloramphenicol Using Bacterially Sensitive Microparticle Loaded Into Dissolving Microneedle: Potential For Enhanced Effectiveness Treatment of Cellulitis

Mukarram Mudjahid, Firzan Nainu, Rifka Nurul Utami, Anwar Sam, Ardiyah Nurul Fitri Marzaman, Tri Puspita Roska, Rangga Meidianto Asri, Achmad Himawan, Ryan F. Donnelly, and Andi Dian Permana*

Cite This: https://doi.org/10.1021/acsami.2c16857

Read Online

ACCESS | Metrics & More | Article Recommendations

**ABSTRACT:** One of the biggest challenges in infectious disease treatment is the existence of bacterial infections in underskin wound tissue, such as cellulitis. Compared to other treatments, it is harder for antibacterial drugs to penetrate the physical barrier on the affected skin with a nonspecific target, making conventional therapy for cellulitis infection more difficult and considered. In this novel research, we pioneer a combined strategy of dissolving microneedles (MNs) and bacteria-sensitive microparticles (MPs) for enhanced penetration and targeted delivery of chloramphenicol (CHL) to the infection site specifically. The polycaprolactone polymer was used to make MPs because of its sensitivity to bacterial enzyme stimuli. The best microparticle formulation was discovered and optimized using the *Design−Expert* application. Furthermore, this study evaluated the antibacterial activity of MPs *in vitro* and *in vivo* on the mutant Drosophila larval infection model. This strategy shows improvement in the antibacterial activity of MPs and higher retention duration compared to conventional cream formulation, and the inclusion of these MPs into dissolving MNs was able to greatly improve the dermatokinetic characteristics of CHL in *ex vivo* evaluation. Importantly, the antimicrobial efficacy in an *ex vivo* infection model demonstrated that, following the use of this strategy, bacterial bioburdens decreased by up to 99.99% after 24 h. The findings offered a proof of concept for the enhancement of CHL dermatokinetic profiles and antimicrobial activities after its preparation into bacteria-sensitive MPs and distribution by MNs. Future research should investigate *in vivo* effectiveness in an appropriate animal model.

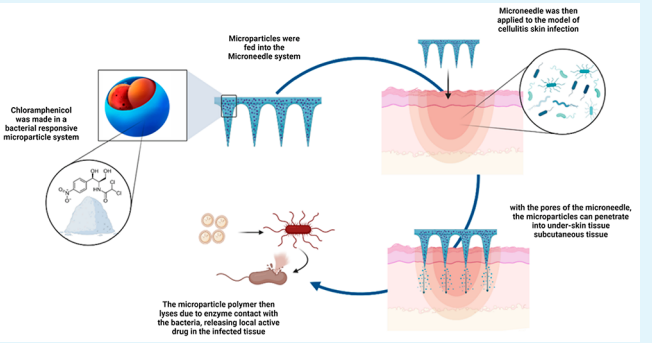


**KEYWORDS:** *bacterially sensitive microparticles, cellulitis, chloramphenicol, dissolving microneedle, polycaprolactone, dermatokinetic*



## 1. INTRODUCTION

Chronic wounds are a major global concern and are typically caused by vascular insufficiency and infection.[1] Infection arises as a result of microorganism growth in the wound site, resulting in a prolonged, excessive inflammatory response, delays in collagen synthesis, and tissue degradation, leading to higher patient mortality and morbidity risks.[1,2] Over $50 billion is spent annually on the management of chronic wounds.[3] Cellulitis is type of chronic wound infection located in the dermis/subcutaneous layer of the skin; it is caused by the immune system's (cytokines and neutrophils) reaction to bacteria penetrating the epidermis.[4,5] The location of the infection in the cutaneous tissue with no visible wound in the epidermis of the skin is often dismissed as ordinary inflammation. These symptoms are also common among the other inflammatory skin diseases, making diagnosis of wound-related cellulitis a substantial challenge at the same time that bacterial cultivation is developing rapidly.[6] It is possible to increase the degree of chronic wounds that were difficult to heal and needed an extension in treatment management.

The primary method for managing infected wounds is surgical debridement, which includes the removal of necrotic and wound tissue. This is usually followed by a regimen of antimicrobial medications for long-term therapy, either topically or systemi-

Received: September 19, 2022
Accepted: November 30, 2022

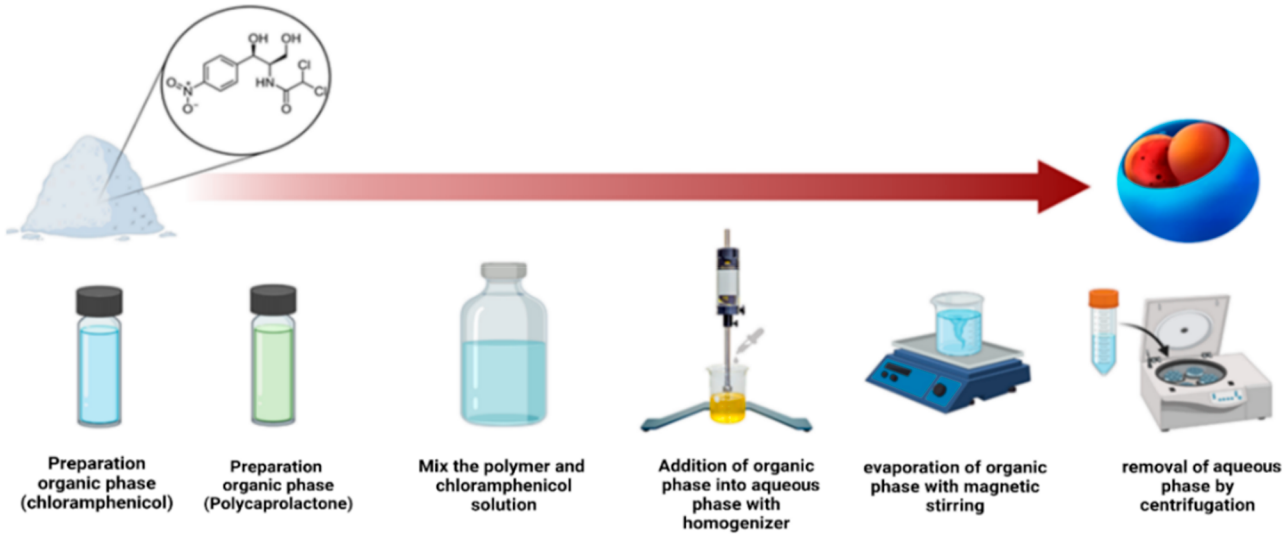


**Figure 1.** Schematic illustration of preparation of CHL-loaded MPs.

cally.[7,8] Additionally, numerous reports of several bacterial strains colonizing human skin tissue have been reported.[9] This is related to the interaction of different strains of bacteria, which can synergistically increase disease severity.[10] Therefore, broad-spectrum antibiotics should be considered when selecting effective treatment. Chloramphenicol (CHL) is a broad-spectrum antibiotic that blocks the peptidyl transferase activity of the bacterial ribosome, which prevents protein chain elongation and inhibits development growth of bacteria.[11] CHL is effective against *Enterococcus faecium* in addition to being a broad-spectrum antibiotic, which has led to its consideration for the treatment of vancomycin-resistant enterococcus.[11,12] However, systemically administered CHL possesses harmful side effects, such as bone marrow damage.[11−13] This is aggravated by the fact that, due to the rise of antibiotic resistance, CHL has recently been given to patients in higher doses.[11] Therefore, it is necessary to create and develop a technique for selective drug administration that can prevent the exposure of CHL to unwanted sites.

Numerous attempts have been previously reported to address this specific problem. Antibiotic delivery, in particular, can be modified by increasing targeting efficiency or reacting to environmental triggers, such as enzyme, pH, or temperature.[14] Natural polymers such as chitosan, cellulose, and albumin are capable of showing both thermal and pH responsive properties, rendering their vast application for drug delivery.[15] However, precise drug release still cannot be completely achieved with these polymers, since the biological pH and temperature fluctuate within a particular range due to individual variances and the degree of infection.[16] Designing a more precise drug release which can only be induced at a very specific environmental trigger can become the solution. For instance, it has been reported that *Staphylococcus aureus* (SA) can produce specifically enzyme like lipolytic esterase. This enzyme can initiate the biocatalytic hydrolysis of a polymer called polycaprolactone (PCL).[17] Given this unique property, PCL can be employed as a suitable material to specifically deliver antimicrobial agents only to the infected tissues. Hence, this approach could prevent exposure to healthy tissues, resulting in a safer therapeutic approach. One of the utilizations of this polymer is the formulation of microparticulate or nanoparticulate delivery system.[18] Small molecules and moderately sized molecules, in the form of micro/nanoparticles, can easily penetrate both the endothelium of the blood and the lymphatic capillary.[19] Particularly for skin delivery, microparticles (MPs) have been shown to retain drugs better than NPs and can help localize long-term drug retention in the skin.[20,21] For that reason, we hypothesize that incorporating chloramphenicol into MPs may enhance their efficiency targeting in skin wound infections.

The effectiveness of the few therapy options for infected wounds is currently limited by toxicity issues and low-to-moderate eschar penetration concerns. Despite the fact that bacterial conjunctivitis has previously been treated with chloramphenicol ointment, there are less data supporting its use in the prevention or treatment of infections in skin wounds.[22] Chloramphenicol is ineffective for the topical treatment of skin infections due to its hydrophobic chemical components,[11] which limit effective cutaneous penetration, as human skin creates an impenetrable barrier that prevents the hydrophobic medication from being transported that way. The issue becomes more significant in the event of an infected lesion, when the medicine should penetrate through the skin around the infection area and improve its therapeutic index.[11] Dissolving microneedles (MNs) are a medication delivery system that may bypass the primary epidermal barrier.[23] MNs can essentially offer a quick, painless, locally focused, and patient-compliant administration strategy.[24] Dissolving MNs, in contrast to hypodermic needle injections, are made of biocompatible polymers and are capable of self-dissolving. Therefore, their use does not result in the production of biohazardous sharps waste.[25] Considering the benefits of this technique, adding MPs to dissolving MNs may enhance the quantity of MPs that reaches the necrotic tissue of infected skin, thereby possibly improving chronic wound infection management for cellulitis.

This study implemented a novel strategy for potentially improving chronic wound treatment from cellulitis by pioneering the production of MPs loaded with CHL and attached in a dissolving MN system. The MPs were evaluated for their structure, antibacterial properties, size, and others physicochemical characterization. To examine the effectiveness of MPs in *in vivo* evaluation, we employed the immunodeficient mutant Drosophila larval model. The release behavior of CHL in MPs


https://doi.org/10.1021/acsami.2c16857
ACS Appl. Mater. Interfaces XXXX, XXX, XXX−XXX

was specifically tested with and without the presence of microorganisms commonly found in chronic infection wounds of cellulitis. The MPs were then added to dissolving MNs, which were evaluated for their insertion and mechanical characteristics. *Ex vivo* infection models in excised infected and normal rat skin were used to explore the *ex vivo* dermatokinetic characteristics of CHL-loaded MPs. Finally, to assess the potential effectiveness of this inquiry, we used an *ex vivo* skin infection model to examine the MPs ability to penetrate and eliminate the burden of bacterial infection.

## 2. EXPERIMENTAL SECTION

**2.1. Materials.** Chloramphenicol (CHL) (purity, 100.00%) was purchased from Merck (Darmstadt, Germany). Polycaprolactone (PCL) (MW 80 000), poly(vinyl alcohol) (PVA) (MW 9000−10 000), polyvinylpyrrolidone (PVP) (MW 40 000), sodium chloride, tryptic soy broth (TSB), potassium chloride, disodium phosphate, and potassium dihydrogen phosphate were obtained from Sigma-Aldrich (Singapore). All other reagents used were analytical grade.

**2.2. Preparation of Chloramphenicol Sensitive Bacterial Microparticles (CHL-Loaded MPs).** Following a previously described procedure with minor modifications, PCL was used as the polymer and PVA as the surfactant to create CHL microparticles using a solvent-evaporation approach.[11] Briefly, PCL was dissolved in 7 mL of chloroform and CHL in 3 mL of methanol. The mixtures were then combined until homogeneous. Then, the polymer−drug mixture was added dropwise into the 25 mL aqueous phase containing 3% PVA as the hydrophilic surfactant under mechanical homogenizer at 500 rpm for 5 min. To ensure the organic phase evaporated entirely, we left the emulsion system under a magnetic stirrer for 5 h. The MPs were then centrifuged to facilitate collection, rinsed three times with distilled water, and dried. Figure 1 illustrates the schematic preparation of CHL-loaded MPs.

**2.3. Optimization of CHL-Loaded MPs through Experimental Design.** CHL-loaded MPs were created using *Design-Expert* (version 13, Stat-Ease, Inc.) by optimizing the crucial process parameters. Following the response surface methodology and central composite design (CCD), three independent variables can influence the characteristics of the resulting MPs: CHL-PCL ratio (*X*1), stirring speed (*X*2), and stirring time (X3). The program carried out 15 runs of formulas for provided values of low and high levels of these factors, denoted by 1 and +1, respectively. These values were also established empirically during preformulation screening. For CHL-loaded MP optimization, dependent variables to be examined included particle size (*Y*1), polydispersity index (PDI) (*Y*2), entrapment efficiency (EE%) (*Y*3), and drug loading (DL%) (*Y*4). Table 1 displays the composition of 15 formulations with the dependent variable outputs.

**2.4. Characterization of CHL-Loaded MPs.** The diameter and polydispersity index (PDI) of CHL-loaded MPs were determined using a microscope (Olympus CS33, Olympus Corporation) and was calibrated using a 10× magnification Optilab camera. Zeta potential of CHL-loaded MPs was determined using a zeta potential analyzer (Brookhaven, New York, USA)

An indirect technique was used to measure the EE of CHL in the MP formulations.[26] After three washing cycles, the free CHL concentration in the supernatant was measured using UV−vis spectrophotometry (Dynamica, HALO XB-10, Dynamica Scientific Ltd., UK). Finally, eq 1 was used to determine the EE of CHL.

$$\mathrm{EE\%} = \frac{\text{Drug Total} - \text{Drug Free}}{\text{Drug Total}} 100\% \quad (1)$$

To determine the DL percentage of CHL in MPs formulations, we dispersed 10 mg of dried MPs into a 7:3 methanol:chloroform mixture, which was placed in sonicator for 1 h to disrupt the MP matrix. Following a 15 min centrifugation at 14 000 rpm of the suspension, the concentration of CHL in the supernatant was determined using a UV−vis spectrophotometer (Dynamica, HALO XB-10, Dynamica Scientific Ltd., UK). Equation 2 was used to calculate the DL percentage.

**Table 1. Composition, Characteristic Design, And Mean of Particle Size, PDI, Entrapment Efficiency (EE), and Drug Loading (DL) of CHL-loaded MPs**

| | independent variables | | | dependent variables | | | |
|---|---|---|---|---|---|---|---|
| run | X1 | X2 (rpm) | X3 (min) | Y1 ($\mu$m) | Y2 | Y3 (%) | Y4 (%) |
| F1 | 1 | 500 | 15 | 17.96 | 0.022 | 41.54 | 22.77 |
| F2 | 1 | 1000 | 10 | 16.40 | 0.018 | 32.74 | 16.37 |
| F3 | 15 | 500 | 15 | 59.46 | 0.030 | 50.82 | 3.17 |
| F4 | 1 | 1500 | 5 | 7.38 | 0.010 | 38.76 | 19.38 |
| F5 | 8 | 1000 | 10 | 49.04 | 0.009 | 44.69 | 4.96 |
| F6 | 8 | 1500 | 10 | 30.34 | 0.010 | 44.31 | 4.92 |
| F7 | 15 | 1000 | 10 | 58.85 | 0.012 | 49.10 | 3.06 |
| F8 | 8 | 1000 | 15 | 38.41 | 0.004 | 37.42 | 4.15 |
| F9 | 1 | 1500 | 15 | 5.82 | 0.389 | 34.55 | 17.27 |
| F10 | 1 | 500 | 5 | 22.37 | 0.010 | 44.41 | 22.20 |
| F11 | 8 | 1000 | 5 | 54.53 | 0.008 | 44.98 | 4.99 |
| F12 | 15 | 1500 | 5 | 55.13 | 0.005 | 49.19 | 3.07 |
| F13 | 15 | 1500 | 15 | 47.10 | 0.007 | 45.46 | 2.84 |
| F14 | 8 | 500 | 10 | 58.68 | 0.012 | 45.56 | 5.06 |
| F15 | 15 | 500 | 5 | 71.26 | 0.013 | 55.70 | 3.48 |

$$\mathrm{DL\%} = \frac{\text{Amount of Encapsulated CHL}}{\text{Total Weight}} 100\% \quad (2)$$

A scanning electron microscope (SEM) was used to examine the morphologies of the CHL-loaded MPs (Hitachi, Krefeld, Germany). A Fourier transform infrared (FTIR) spectrometer (Accutrac FT/IR-4100TM Series, Jasco, Essex, UK) was used to examine the chemical interactions between each component in the formulas. A differential scanning calorimeter was used to conduct thermal profile investigation of CHL, polymers, physical mixtures, and CHL-loaded MPs (DSC 2920, TA Instruments, Surrey, UK). An X-ray diffractometer instrument was used to perform crystalline profile diffraction on CHL and CHL-loaded MPs (Rigaku Corporation, Kent, England).

**2.5. Hemolytic Activity of CHL-Loaded MPs.** In this investigation, the hemolysis potential of the cells may be utilized to evaluate the biocompatibility and safety of the designed drug delivery system. Following a previously described procedure, an *in vitro* hemolytic experiment was carried out to evaluate the hemolytic activity of CHL-Loaded MPs.[27] Briefly, erythrocytes were collected from the blood of healthy female Sprague−Dawley rat by centrifugation at 2000 RCF for 10 min. The blood was then washed with PBS and processed to three cycles of centrifugation under the same conditions. The erythrocytes were washed and resuspended in PBS to a final concentration of 10% v/v. Nine-hundred microliters of samples containing CHL and CHL-loaded MPs were diluted in PBS until they reached 5, 50, and 500 $\mu$g/mL concentrations. Then, 100 $\mu$L of the produced cell (erythrocytes) suspension was added. After that, the mixtures were centrifuged at 14 000 RCF for 10 min after being incubated at 37 °C for 60 min. Finally, to determine the amount of free hemoglobin, we used UV−visible spectroscopy to measure the absorbance of the supernatant (Dynamica, HALO XB-10). Accordingly, PBS and distilled water were used as negative and positive hemolytic controls. When assessing the hemolysis of the samples, a change in the color of sample mixture was also seen. For each concentration, the experiment was run in three replications. Equation 3 was used to determine the hemolysis percentage:

$$\mathrm{Hemolysis(\%)} = \frac{\mathrm{OD(Test\ sample)} - \mathrm{OD(Negative\ control)}}{\mathrm{OD(Postive\ control)} - \mathrm{OD(Negative\ control)}} 100\% \quad (3)$$

**2.6. *In Vitro* Antibacterial Activities.** *2.6.1. Culture of Bacterial Strains.* The microorganism employed in this investigation was SA ATCC 25923. The strains were purchased from LGC Standards in Middlesex, UK, kept at 4 °C, and were subcultured on new media at regular intervals. Before each antibacterial experiment, the bacterial


https://doi.org/10.1021/acsami.2c16857
ACS Appl. Mater. Interfaces XXXX, XXX, XXX−XXX

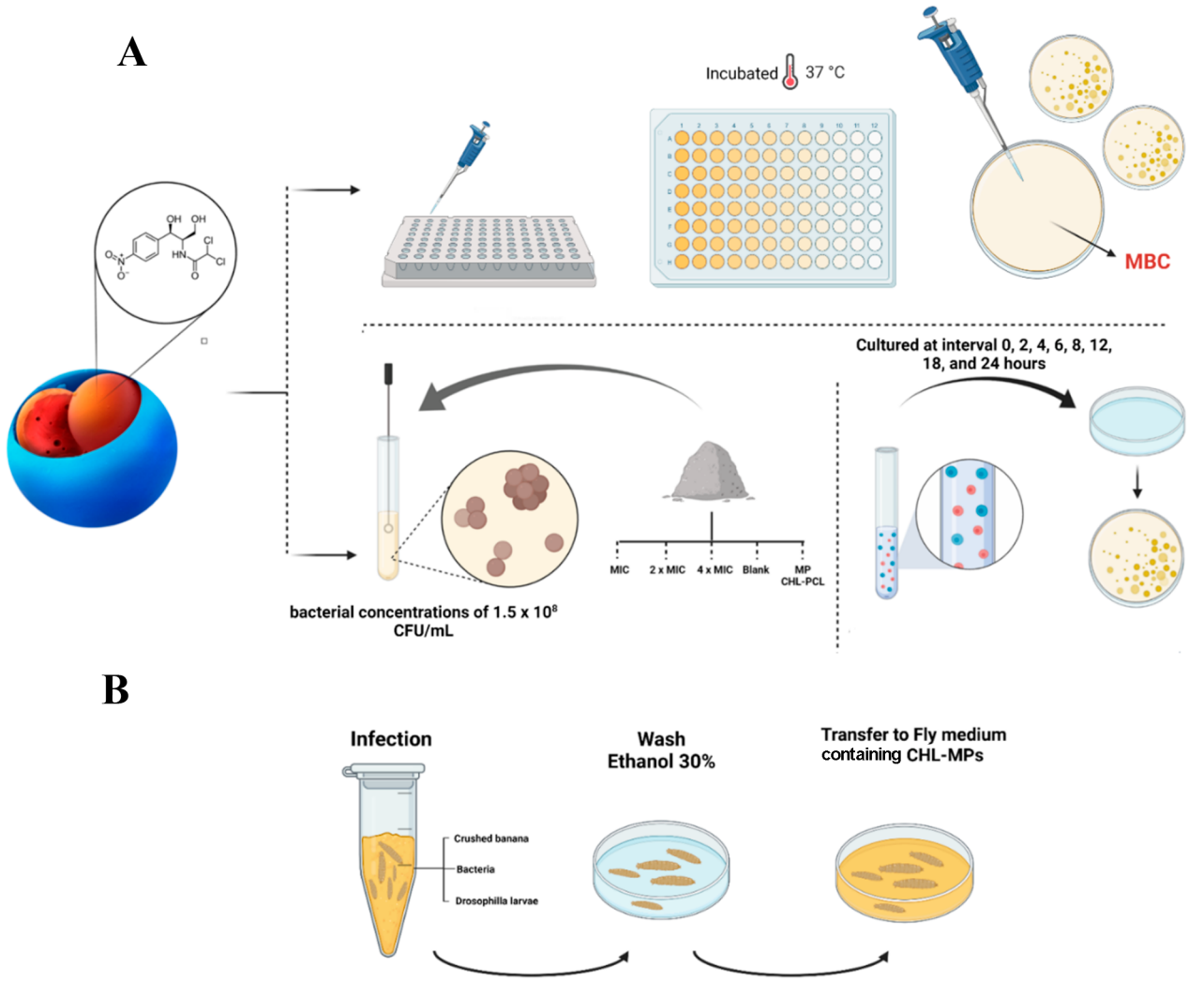


**Figure 2.** Schematic illustration of (A) MIC, MBC, and time kill assay and (B) infection experiment on Drosophila larva infection model.

strains were cultured overnight and incubated at 37 °C in TSB media. Serial dilutions with TSB were used to create inoculums of bacteria (placing the diluted mixture on tryptic soy agar (TSA) plates allowed for the accurate counting of bacteria), resulting in final concentrations of $1.5 \times 10^8$ colony forming units (CFU)/mL.

*2.6.2. Determination of Minimum Inhibitory Concentration and Minimum Bactericidal Concentration.* As previously described, a microtiter broth dilution technique was used to determine the minimal inhibitory concentrations (MICs) and minimal bactericidal concentrations (MBCs) of CHL and CHL-loaded MPs in 96 well bottom plates.[28] Various concentrations of CHL and CHL-loaded MPs (3.125−200 $\mu$g/mL) were used to calculate the MIC in TSB along with the corresponding equilibrated concentrations of chloramphenicol. Each tube received a 100 $\mu$L volume of each bacterial inoculum, which was then cultured for 24 h at room temperature (see Figure 2a). The positive and negative controls utilized were TSB and TSB with bacteria, respectively. The lowest concentration of the tested substance, which had no visible growth after 24 h of incubation, was considered the MIC.

MBC was calculated by cultivating 20 $\mu$L on TSA plates and incubating them at 37 °C for 24 h in wells corresponding to the MIC and the above-mentioned dilutions. The researchers then determined how many bacterial colonies were present on the plates. The MBC was determined to be the lowest concentration that inhibited 99.9% of bacterial growth. Equation 4 was used to determine the killing percentage

$$\text{Killing percentage}(\%) = \frac{\text{CFU(Control)} - \text{CFU(Experiment)}}{\text{CFU(Control)}} 100\% \quad (4)$$

*2.6.3. Time Kill Assay.* Following the procedure outlined before described, the time-killing kinetics of CHL and CHL-loaded MPs against SA was determined.[29] MPs loaded with CHL were created and added to the bacterial suspensions ($1.5 \times 10^8$ CFU/mL). CHL doses corresponding to MIC, 2× MIC, and 4× MIC were also prepared and applied. Then, 37 °C of incubation was applied to the bacterial cultures. Twenty $\mu$L aliquots from the cultures were obtained at intervals of 0, 2, 4, 6, 8, 12, 18, and 24 h and aseptically injected on TSA plates. To calculate the bacteria's viable CFU, the plates were incubated for 24 h at 37 °C. The procedure was performed in triplicate, and a log CFU/mL vs time kill curve was constructed. Figure 2a illustrates the schematic time kill assay.

**2.7. *In Vivo* Antibacterial Activities in Drosophila Larval Model.** *2.7.1. Bacterial Strains and Fly Stocks.* SA ATCC 25923 was the bacterial strain used as the infecting agent. It was purchased from LGC Standards in Middlesex, UK, and kept at 4 °C. Bacteria were cultivated separately in TSB medium and incubated at 37 °C. When the cultures had grown to their maximum potential, they were collected, rinsed with PBS, and employed in the tests. This study used the psh[1];;modSP[KO] Drosophila line, which is an immunodeficient fly line that lacks Toll pathway activity. All flies were kept on conventional cornmeal-agar medium at a temperature of 25 °C.


https://doi.org/10.1021/acsami.2c16857
ACS Appl. Mater. Interfaces XXXX, XXX, XXX−XXX

*2.7.2. Infection Experiment.* The infection experiment on larval Drosophila was carried out as previously described with minor modifications.[30] Two and a half days after eggs were laid, the researchers began infecting mid-L2 larvae. Animals were put in a 1.5 mL microcentrifuge tube for 30 min per test, along with 300 $\mu$L of crushed bananas and 300 $\mu$L of an overnight bacterial culture (See Figure 2b). A foam stopper was used to obstruct the animals, ensuring that they stayed at the bottom of the tube for the duration of the infection. Upon completion of this stage, they were quickly cleaned in 30% ethanol before being put on a Petri dish with a new fly medium free of yeast and containing CHL-loaded MPs. Waiting durations and infections were conducted at 29 °C.

**2.8. *In Vitro* Release Study of CHL-Loaded MPs in Bacterial Cultures.** The *in vitro* release study of CHL-loaded MPs in bacterial cultures was determined. The release tests of CHL and CHL-loaded MPs were carried out in the presence or absence of bacteria in fluid mimicking infection media.[17] Briefly, MPs with a CHL equivalent of 50 mg were dissolved in 50 mL of the bacterial cultures and incubated at 37 °C and 100 rpm in an orbital shaker. At 0.25, 0.5, 0.75, 1, 2, 3, 4, 5, 6, 7, 8, and 24 h of incubation, samples from the cultures were taken out and inoculated on TSA plates with the proper dilutions. At predetermined intervals, 0.5 mL aliquots of the sample were removed and filtered. The concentration of CHL in the filtrate was measured using a spectrophotometer UV−vis.

To assess the kinetic release profiles, we used DDSolver (China Pharmaceutical University, Nanjing, China)[31] to fit in five mathematical models, including zero-order kinetics (ZO), first-order kinetics (FO), Higuchi, Korsmeyer−Peppas (KP), and Hixson−Crowell (HC).

$$\text{Zero-Order Kinetics: } C_t = C_0 + k_0 t \tag{5}$$

$$\text{First-Order Kinetics: } \ln C_t = \ln C_0 + k_1 t \tag{6}$$

$$\text{Higuchi Model: } C_t = k_H \sqrt{t} \tag{7}$$

$$\text{Korsmeyer−Peppas Model: } C_t = k_{KP} t^n \tag{8}$$

$$\text{Hixson−Crowell Model: } C_t^{1/3} = C_0^{1/3} k_{HC} t \tag{9}$$

$C_t$ denotes the concentration of CHL at period $t$, $C_0$ indicates a primary combination of CHL in-side of medium ($t = 0$), $K_0$, $K_1$, $K_H$, $K_P$, and $K_{HC}$ were the coefficients of release of the relevant kinetic models. A calculation from every type will be explained and the fit of release kinetics was selected by a reciprocity of coefficient ($r^2$).

**2.9. Formulation Design and Manufacture of CHL-MP-Loaded Dissolving Microneedle (MNs).** A two-step manufacturing procedure was used to create two-layered dissolving MNs, with a few minor modifications.[20,25] The polymer solutions were mixed with the ratio depicted in Table 2. The same quantity of CHL-loaded MPs

**Table 2. Composition of Formulations MNs Containing CHL-Loaded MPs**

| | concentration (%b/b) | | | |
|---|---|---|---|---|
| formulas | MPs | PVP | PVA | Aquadest |
| **F1** | 25 | 20 | 15 | 40 |
| **F2** | 25 | 20 | 20 | 35 |
| **F3** | 25 | 20 | 25 | 30 |
| **F4** | 25 | 25 | 20 | 30 |
| **F5** | 25 | 15 | 20 | 40 |

pellets was combined with the polymer mixture to create the MN formulation. They were then exposed to sonication to achieve a clean bubble-free dispersion. Then, 50 mg of the mixture was poured into the silicone MN molds. The polymer−drug combination was then put on the mold and centrifuged. Following centrifugation, the extra polymer mixture at the top of the mold was extracted and replaced using a spatula; the formulas were kept at room temperature for 4 h. Following that, the two-layered MNs were created by pouring an aqueous gel containing blank polymer mixtures. Then, the molds were centrifuged again. The produced MNs were then dried for 24 h at room temperature and 24 h at 37 °C without being removed from the mold (See Figure 3). In addition to MNs with CHL-loaded MPs, MNs with free CHL were generated for additional research using the same procedure. Figure 3 is schematic illustration of manufacturing the two-layered MNs.

**2.10. Mechanical Strength and Penetration Ability Test.** To assess the MN response after applied pressure, we carried out mechanical strength and penetrating ability tests using the previously stated approach with minor modifications.[32] This assessment was done by measuring the MN capacity penetration through eight layers of parafilm, which was the same thickness as the top layer of human skin. Pressure (30 N) was used to apply the MNs for 30 s. A weight of 3.06 kg was placed on top of the microneedles to create this pressure. It is important to note that during the trial, equal pressure was applied to all sides of the MNs. Then, the number of holes in each layer of parafilm was counted and MN size and shape were examined under a microscope in accordance with technique described previously.[33] The following calculations are used to compute the proportion of mechanical strength and MN penetration capability.[34]

$$\text{compression\%} = \frac{\text{initial height} - \text{height after pressure applied}}{\text{initial height}} 100\% \tag{10}$$

$$\text{\%penetration of } n \text{ layer} = \frac{\text{no. of holes in } n \text{ layer}}{\text{total no. of holes}} 100\% \tag{11}$$

**2.11. Calculation of Drug Content Localized to the Needles.** To quantify the amount of CHL in MNs, needle MNs were scraped carefully from the baseplate using a scalpel and then dissolved in 5 mL of distilled water. Methanol: chloroform mixture with ratio of 7:3 (2 mL) was added to the dispersion and placed in sonicator for 1 h to disrupt the MP matrix. Following a 15 min centrifugation at 14 000 rpm of the suspension, the concentration of CHL in the supernatant was determined using a spectrophotometer UV−vis (Dynamica, HALO XB-10, Dynamica Scientific Ltd., UK)

**2.12. Stability Test of MP-CHL Loaded into MNs.** MNs containing CHL-loaded MPs were kept in static storage at 25 °C. The initial sizes, PDIs, EE, DL, and zeta potentials were compared to those obtained in 10 days and storage at 25 °C to determine stability. The statistical analysis was used to assess the significance stability of MPs.

**2.13. Dissolution Study, *Ex Vivo* Dermatokinetic Studies, and Anti-Infection Activity in *Ex Vivo* Model of Infection on Rat Skin.** *2.13.1. Preparation of Ex Vivo Model of Infection on Rat Skin.* Wistar rats' abdomen skins were removed and placed in PBS before the experiment (pH 7.4). Rat skins were washed in ethanol at a 70% concentration for 1 h. The skins were kept in a biosafety cabinet for 20 min to allow the ethanol to evaporate before wounding the surface 5 mm with a biopsy punch (Stiefel, Middlesex, UK). The previously reported procedures were then applied to develop *ex vivo* models of infection on rat skin, with a few minor modifications.[35] After wounding and infection, the skins were transferred on TSA plates and 50 $\mu$L of the diluted bacterial suspension ($1.5 \times 10^8$ CFU/mL) were equally injected to the wound of the skin. Every day for 5 days, the skins were moved to new TSA media plates, which were then incubated at 37 °C to encourage the formation of the infection.

*2.13.2. Dissolution Study.* The MNs dissolution study was assessed in an *ex vivo* model of skin infection. Briefly, the MN arrays were physically implanted into the epidermal area, and a 5.0 g cylindrical stainless-steel weight was placed on top to guarantee the array stayed in place. MN arrays were collected at various interval time points and examined using a Leica EZ4 D stereo microscope.

*2.13.3. Ex Vivo Dermatokinetic Studies.* *Ex vivo* dermatokinetic tests of MNs containing free CHL and CHL-loaded MPs were performed on excised full-thickness skin in both infected and infection models. This investigation was conducted using the previously outlined methodology.[23,25] Initially, cyanoacrylate glue was used to affix the skin to the franz cell diffusion cells' donor compartment. The receiver chamber with PBS was coupled with another donor compartment., and the MNs were manually forced into the skin for 30 s (pH 7.4). The MNs


https://doi.org/10.1021/acsami.2c16857
ACS Appl. Mater. Interfaces XXXX, XXX, XXX−XXX

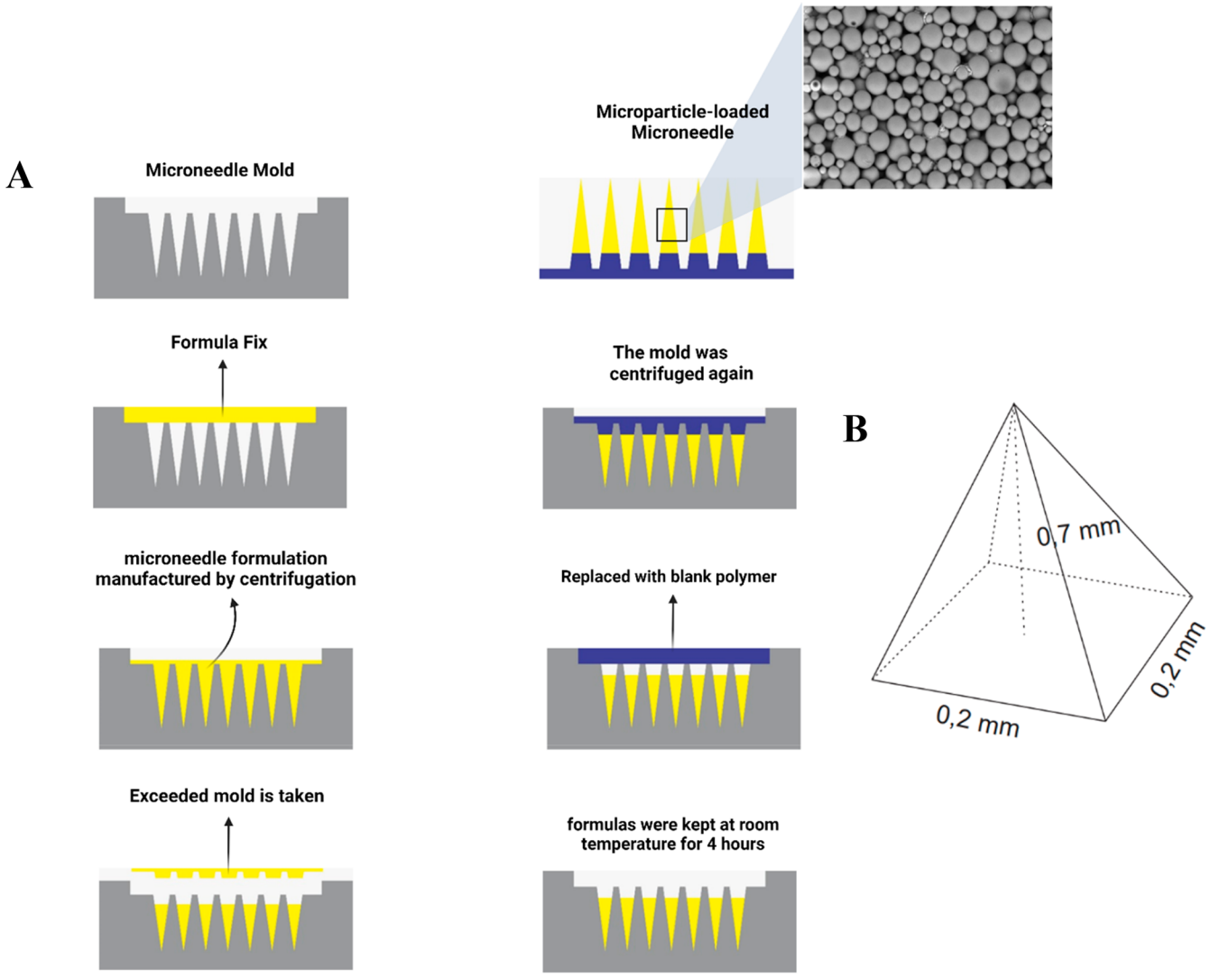


**Figure 3.** (A) Two-layer dissolving MN manufacturing scheme, (B) MN dimensions.

were kept in place during the experiment by a cylindrical stainless steel mass that weighed 5 g. The recipient compartment's temperature was maintained at 37 ± 1 °C, and Parafilm was employed to seal the donor compartment and sampling side. At 600 rpm, the compartment was agitated. At regular intervals (1, 2, 3, 4, 5, 6, 8, and 24 h), the MNs were taken, and the skin was then three times washed with sterile water. To extract the CHL released in the skin, the skin sample was then collected and the surface was cleaned with distilled water. After cleaning, the skin sample was cut into small pieces and 2 mL of PBS was added to extract CHL from the tissue. The sample was then vortexed for 5 min and centrifuged at 14 000 rpm for 15 min. The supernatant was analyzed using a UV−vis spectrophotometer instrument (Dynamica, HALO XB-10, Dynamica Scientific Ltd., UK).

To assess the dermatokinetic profiles, PKSolver (China Pharmaceutical University, Nanjing, China),[31] was used in a one-compartment open model. We calculated the drug concentration time curve from time zero ($t = 0$) to the end experimental time point ($t = 24$ h) (AUC), the mean half-life ($t_{1/2}$), the mean residence time (MRT), the maximum drug concentration in skin ($C_{max}$), and the time of maximum concentration ($t_{max}$). To ensure that the skin extraction method was only able to remove the CHL released from MPs without harming the MPs, we applied the extraction method to the CHL-loaded MPs dispersion, and processed using the same steps. It should be noted that the extraction method did not affect the CHL encapsulated in the MPs. Comparative investigations were carried out utilizing MPs that were loaded with specific amounts of CHL and needle-free patches conveying free CHL.

*2.13.4. Antimicrobial Activity in Ex Vivo Model of Infection on Rat Skin.* The technique previously described,[35,36] was used to measure anti-infection activity, with a few minor modifications. Twenty microliters of the supernatant from dermatokinetic experiments 24 and 48 h after application time was inoculated onto TSA plates and was incubated for 24 h at 37 °C to assess the anti-infection effectiveness of MNs formulation loaded with CHL and MPs-CHL in an *ex vivo* model. Additionally, the same procedure was carried out using cream containing CHL and CHL-loaded MPs on the diseased skin. Finally, the number of viable CFUs was determined. Normal skin was utilized as a negative control, while infected skin was used as a positive control without MN treatment.

**2.14. Statistical Analysis.** The findings of the experiment were presented as means and standard deviations (SD) of the means. GraphPad Prism version 6 was used (GraphPad Software, San Diego, California, USA) for statistical analysis. An unpaired $t$ test was employed to compare the two groups. In addition, the Kruskal−Wallis test with a posthoc Dunn's test was utilized to compare different groups. Statistical significance is indicated by a value of $p < 0.05$.

## 3. RESULTS AND DISCUSSION

**3.1. Formulation of CHL-Loaded MPs.** The solvent-evaporation approach was used to prepare CHL-loaded MPs,


https://doi.org/10.1021/acsami.2c16857
ACS Appl. Mater. Interfaces XXXX, XXX, XXX−XXX

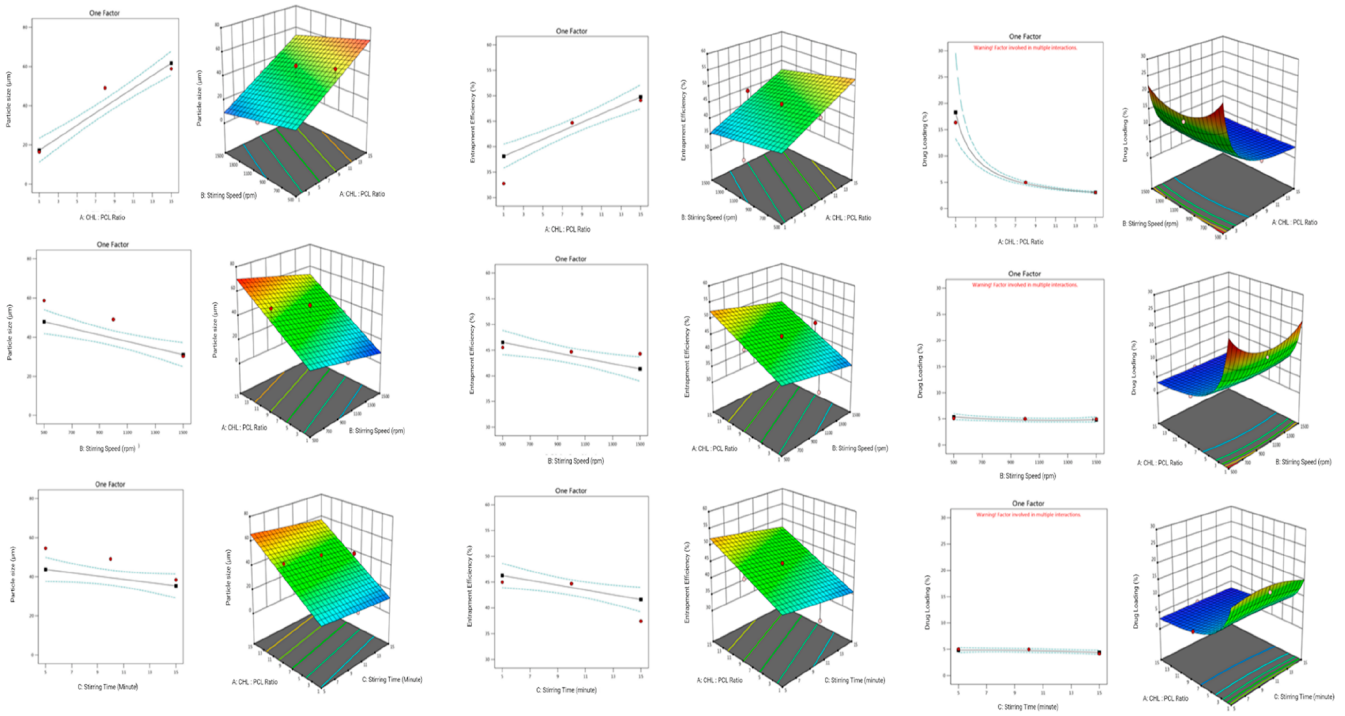

**Figure 4.** 2D and 3D response surface graphs displaying the impact of independent factors on (A) particle size, (B) EE%, and (C) DL%.

because this approach is suitable for producing MPs containing hydrophobic compounds such as CHL.[11] The initial issue was choosing an organic phase that could dissolve both chloramphenicol and the polyester polymer, PCL. A mixture of methanol and chloroform solvent with a ratio of 7:3 was used to create CHL-loaded MPs because these solvents mixed well and homogeneously (i.e., clear), and no harmful chlorinated organic solvents were used to incorporate the drug into the MPs. The cosolvent was also employed to aid in the solubility of CHL, which was then integrated into the hydrophobic core of CHL-loaded MPs.

**3.2. Statistical Analysis of Experimental Data by *Design-Expert* Software.** A total of 15 formulations with various level of ratio CHL:PCL ($X1$), stirring speed ($X2$), and stirring time (X3) were successfully formulated and screened using CCD under *Design-Expert* (version 13, Stat-Ease, Inc., Minneapolis, USA). The best mathematical model was selected based on statistical goodness-of-fit including $F$-value, predicted and adjusted $R$-squared values, and adequate precision. After confirming the model significance in terms of an analysis of variance test with a $p$-value of 0.05 or below, the data were evaluated. The impact of each independent variable on different answers was calculated after critical analysis.

*3.2.1. Effect of Independent Variables on Particle Size.* The physicochemical characteristics (e.g., drug loading, release profile, bioavailability) and physiological behavior (e.g., interaction with plasma components, phagocytosis, uptake) of MPs are commonly dependent on particle size.[37] The 15 formulations tested in this study had mean particle sizes between 5.82 and 71.26 $\mu$m (Table 1), which is ideal for skin penetration and retention.[20] Compared to the quadratic and two-factor models, the linear model, with an $R$-squared value of 0.9196 and an adjusted $R$-squared value of 0.8976, was determined to be the best match for answer Y1. ANOVA was used to assess the linear model's significance for the quantitative impacts of variables on response. The linear model had a significant ANOVA result ($p < 0.05$) and a model $F$-value of 41.92. The signal-to-noise ratio is measured by "Adeq Precision," and a value greater than 4 is preferred.[38] The calculated ratio, 19.827, suggested that the anticipated model would be helpful in guiding the design space. An empirical polynomial equation based on data analysis was produced and is represented by the following coded factors:

$$\text{Mean particle size } (\mu\text{m})\ Y1 = +39.34292 + 3.16933X1 - 0.016791X2 - 0.838608X3 \quad (12)$$

Regarding the ANOVA results, CHL:PCL Ratio ($X1$) and stirring speed ($X2$) had a significant impact on particle size. According to Equation 12, the significant positive coefficient for $X1$ indicated that the particle size significantly increased with increasing polymer concentration ($p < 0.05$). This can be explained by the fact that when polymers are more highly concentrated, there are more interactions between particles during emulsification. This causes the fusing of partially formed particles, which in turn causes an increase in particle size.[39] Additionally, increasing polymer content increases the organic phase's viscosity, which finally slows down its diffusion into the aqueous phase and produces bigger microparticles.[40] Further, the significant negative coefficient for $X2$ indicated that the particle size significantly decreased with increasing stirring speed ($p < 0.05$). This is because emulsification at fast speed can lead to a reduction in emulsion globules; as a result, a lower emulsion globule size permitted the production of smaller microparticles. As homogenization proceeds more quickly, more energy is released, which causes the polymeric organic phase to disperse more quickly and produces small microparticles with monomodal distributions. The values of the $X2$ and $X3$ coefficients were negative, indicating an inversely proportional effect with the resulting particle size response. However, stirring time coefficients for $X3$ were not significant ($p > 0.05$).


https://doi.org/10.1021/acsami.2c16857
ACS Appl. Mater. Interfaces XXXX, XXX, XXX−XXX

Two variables can have simultaneous impacts, which can be shown in 3D surface plots. Plot $X1 \times 2$'s curved shape showed that the factors strongly interacted to affect particle size. Although CHL:PCL ratio and stirring speed are clearly correlated to particle size, these relationships are not statistically significant ($p > 0.05$) based the positive coefficient value for stirring time ($X3$). As seen in Figure 4A, two and three-dimensional surface plots vividly demonstrate how numerous independent factors affect particle size. The intensity of the red hue indicates an increase in particle size with corresponding changes CHL:PCL ratio, stirring speed, and stirring time

*3.2.2. Effect of Independent Variables on Polydispersity Index.* The polydispersity index (PDI) is a value that describes sample heterogeneity by size distribution. Polydispersity can occur due to size distribution in the sample or agglomeration and aggregation of samples during the synthesis and analysis process. Size heterogeneity will cause fluctuations in the amount of drug that penetrates and is retained in the skin. In this study, the average PDI value is below 0.05, which indicates a monodispersed system. Based on the results of the analysis, there is no mathematical model that follows the trend of good PDI values. The ANOVA test results also showed a data trend that was not significant ($p > 0.05$). This suggests that none of the independent variables—polymer ratio ($X1$), stirring speed ($X2$), or stirring time ($X3$)—significantly affected the PDI values.

*3.2.3. Effect of Independent Variables on EE Percentage.* To achieve the necessary bactericidal activity, MPs must have the capacity to encapsulate a sizable quantity of CHL. Table 1 shows the EE percentage achieved for CHL, which ranged from 32.74 to 55.70%. A linear model with R-squared of 0.8589 and adjusted R-squared of 0.8204 was determined to be the best match for response Y2 when compared to quadratic and two-factor models. The linear model is significant according to the ANOVA test ($p < 0.0001$), and the model's $F$-value is 22.32, meaning that there is only a 0.01% possibility of mistake. Additionally, a low CV value of 5.96% clearly indicated a high level of accuracy and dependability of the experimental data. The Adeq precision number (15.850) showed the effectiveness of the anticipated model for navigating the design space. Based on data analysis, the EE equation is presented below.

$$\text{Entrapment Efficiency (\%) } Y3 = +47.09142 + 0.832379X1 - 0.005147X2 - 0.464984X3 \quad (13)$$

According to the ANOVA results, the linear coefficients ($X1$, $X2$, and $X3$) with $p$-values 0.05 substantially impacted the EE percentage. The positive coefficient for $X1$ in eq 13 demonstrates that as the concentration of hydrophobic polymer increases, EE increases ($p < 0.05$), which may be explained by the hydrophobicity of CHL and its higher miscibility in the organic phase. Previous research has noted this pattern for hydrophobic medicines, indicating that enhanced interactions with polymeric solutions and increased organic phase consistency diminish drug partitioning in the aqueous phase, leading to higher MP encapsulation.[41]

Regarding the other parameter coefficient, the negative coefficient for $X2$ and $X3$ indicated that entrapment efficiency significantly increased with decreased parameter speed and time of Stirring ($p < 0.05$). This may be due to the higher speed and longer time of homogenization; more energy is released in the process that leads to a rapid dispersion of polymeric organic phase. As a result, the entrapment process becomes shorter, and more drug is released in the polymer matrix, thereby reducing the entrapment efficiency. Surface graphs in two and three dimensions clearly show how different independent factors affect the EE% (Figure 4B). The intensity of the red hue corresponds to an increase in the EE% with the corresponding changes in changes of the CHL:PCL ratio, stirring speed, and stirring time.

*3.2.4. Effect of Independent Variables on DL Percentage.* DL is the process of incorporation of a drug into a carrier system. The DL percentage for CHL, which varied from 2.84 to 22.77%, is shown in Table 1. In comparison to linear and two-factor models, a quadratic model with an $R$-squared value of 0.9971 and an adjusted $R$-squared value of 0.9918 was found to be the best fit for answer $Y4$ (DL). According to the ANOVA test, the quadratic model is significant ($p < 0.05$), and the model's $F$-value is 190.29, implying that there is only a 0.01% chance of error. Additionally, a low CV value of 5.37% made it abundantly evident that the experimental results had a high degree of dependability and accuracy. Adeq Precision is parameter that measures the signal-to-noise ratio. A ratio greater than 4 is desirable. This study obtained a ratio of 36.367, indicating adequate signal and showing that the expected model was very useful for traversing the design space. Based on data analysis, the final equation is shown below.

$$\text{Drug Loading (\%) } \frac{1}{Y4} = +0.000729 + 0.021958X1 + 0.000104X2 - 0,005387X3 - 0.000402X1^2 \quad (14)$$

According to the ANOVA results, the CHL:PCL ratio ($X1$), stirring speed ($X2$), and stirring time ($X3$), and the polynomial models of CHL:PCL ratio ($X1^2$) were significant ($p < 0.05$). However, the remaining term coefficients were not significant ($p > 0.05$). Based on eq 14, the positive coefficient for X1 is associated with the $1/Y4$ value indicating that the drug loading decreased significantly with increasing CHL:PCL ratio ($p < 0.05$). this phenomenon is the same as previously described regarding the entrapment efficiency by the hydrophobicity of CHL and higher miscibility in the organic phase. Thus, the enhanced interaction with the polymer solution and the increased consistency of the organic phase reduced drug partitioning in the aqueous phase, leading to higher MP encapsulation. However, the increase in the CHL:PCL ratio will increase the weight of the microparticles, thereby also decreasing the DL value.

The positive coefficient for $X2$ when associated with variable $1/Y4$ values indicates that drug loading decreases significantly with increasing stirring speed ($p < 0.05$). This phenomenon is similar to the one previously described. This may be due to the higher speed and longer homogenization time; more energy is released in the process, which leads to the fast dispersion of the polymer organic phase. As a result, the entrapment process becomes shorter, and more drug is released into the polymer matrix, thereby reducing the entrapment efficiency and resulting in a reduced DL value. However, this is different from the $X3$ parameter. The negative coefficient for $X3$ when associated with variable values indicates that drug loading increases significantly with longer stirring time ($p < 0.05$). Surface graphs in two and three dimensions clearly show how different independent factors affect the DL% (Figure 4C). The intensity of the red hue corresponds to an increase in the DL% with the corresponding changes in CHL:PCL ratio, stirring speed, and stirring time.


https://doi.org/10.1021/acsami.2c16857
ACS Appl. Mater. Interfaces XXXX, XXX, XXX−XXX

**3.3. Optimization and Validation.** Following analysis of polynomial equations with independent and dependent variables, additional optimization and validation were performed. The optimal formula solution for CHL-loaded MPs creation with desired properties was obtained for this purpose by using design expert software (minimum for particle size and PDI and maximum for EE and DL). The improved formulation had a 1:1 of CHL to PCL, a stirring speed of 500 rpm, and 5 min of stirring time. The projected values of particle size (Y1), polydispersity index (PDI) (Y2), entrapment efficiency (EE%) (Y3), and drug loading (DL%) (Y4) at these levels were 29.697, 0.012, 42.955, and 23.283, respectively. These values had a desirability of 0.647 (i.e., having a 64.7% chance of producing the predicted results in terms of dependent variable). CHL−loaded MPs were then created using the recommended ideal values, and the projected model's accuracy was checked. The validity of the CCD used to generate the necessary CHL-loaded MPs formulation was proven by the minimal variance between theoretical predictions and actual outcomes.

**3.4. Physicochemical Characterization of Optimized MP CHL−PCL Formulation.** The breadth of the size distribution and subsequent medication penetration through the skin are determined by both particle size and PDI. The predicted and observed response variables of the optimal manufacturing CHL-loaded MPs can be seen in Table 3. The

**Table 3. Predicted and Observed Response Variables of the Optimal Manufacturing CHL-Loaded MPs**

| | Y1 | Y2 | Y3 | Y4 |
|---|---|---|---|---|
| predicted | 28.59 | 0.011 | 42.61 | 21.53 |
| observed | 24.33 | 0.010 | 40.96 | 19.12 |
| predicted error (%) | 14.89 | 8.727 | 3.87 | 11.19 |

24.33 $\mu$m particle size of the optimized CHL-loaded MP formulation was consistent with the expected value (28.595 $\mu$m). The 0.010 PDI value obtained was also consistent with the expected value (0.011), showing that the formulations were monodisperse and homogeneous. Figure 5D shows the morphologies of CHL-loaded MPs as seen by SEM. SEM scans revealed that all formulations had spherical shapes. Regarding the other parameters, the most crucial factors affecting MPs' desired therapeutic action were entrapment efficiency and drug loading. EE and DL percentages of 40.96 and 20.48%, respectively, were displayed by optimized CHL-loaded MPs, which were close to the expected values of 42.61 (EE) and 21.53% (DL). Based on the validation findings, the results align with the predicted value with a bias level below of 15%.

The zeta potential measurement for microparticles (MPs) was $-7.54 \pm 0.65$ mV. The presence of the ionized carboxylic groups of PCL was the cause of the negative zeta potentials observed for MPs.[42] The amount of MPs adhering to the bacterial cell surface of SA corresponds closely with the values of zeta potential difference.[43] It has been previously reported that the zeta potential value of SA was −35.6 mV.[44] As a result, it is possible to infer that the higher of zeta potential difference between SA and MPs as a straightforward and brief description of the good adsorption mechanism in bacteria-MPs systems.

To confirm that there had been no chemical interactions between CHL and the ingredients used to create MPs, FTIR analysis was employed. Chloramphenicol's characteristic infrared peaks show the existence of a free hydroxyl group, N−H stretching, aromatic stretching, $CH_2$ asymmetric and symmetric stretching, and C−O stretching.[11] Figure 5A displays the FTIR spectra CHL, and CHL-loaded MPs. The CHL spectrum display had absorption peaks of 3487 OH stretching vibration, 3218 NH stretching vibration, 2978 aromatic C−H stretching vibration, 1686 C═O stretching vibrations, and 1549 $NO_2$ stretching peak. These peaks are similar to those reported in previous investigations.[22] It has been concluded there were no chemical interactions between CHL and the components used to generate CHL-loaded MPs, and all of the characteristic CHL peaks were identical in the MPs, demonstrating the existence of all key functional groups of CHL.

Figure 5B displays the differential scanning calorimetry (DSC) analysis findings for CHL and CHL-loaded MPs. Because CHL crystals have melting temperatures around 148 °C, the data exhibited pronounced endothermic peaks. However, with CHL-loaded MPs, this peak was not seen. Figure 5C shows the XRD diffractograms of the pure CHL and its MP formulations. Due to the strong crystalline features of CHL, sharp characteristics peaks of CHL were seen at $2\theta$ values from 15 to 24. The spectra obtained are the same as the results reported in previous studies.[11] These peaks, however, were not visible in MPs formulations, which is identical to the findings of the DSC investigation. The total encapsulation of CHL in amorphous or solution form in the MP polymers utilized in this work may be the source of the lack of the CHL peak in the DSC and XRD analyses. However, the lack of the CHL peak did not affect the pharmacological activity of CHL, which is in agreement with FTIR results that showed all of the characteristic CHL peaks were identical in the MPs, demonstrating the existence of all key functional groups of CHL.

**3.5. Hemolytic Activity of CHL-Loaded MPs.** Hemolytic activity study in mammalian erythrocytes is used to assess antimicrobials' bacterial selectivity of toxicity. According to our investigation, the hemolysis value for MPs was 0% through measurements using the spectrophotometric method. It has also seen by clearer and more translucent erythrocyte cells that have been measured after MP therapy and compared to the positive control (distilled water) (see Figure 5E). Manufacturing CHL-loaded MPs did not exhibit significant hemolysis (5%) in any of the tested doses (5, 50, and 500 ppm). The results showed that MP compositions are safe to use since hemolysis indices lower than 5% are considered safe.[45]

**3.6. *In Vitro* Release Kinetic Study of CHL-Loaded MPs.** Studies on kinetical drug release provide the information on how long a drug substance stays in the system. The kinetical release study of CHL and CHL-loaded MPs was conducted in both the absence and presence of the bacteria in several media (see Figure 6). We chose PBS as the initial kinetics media for investigation because it reflects typical skin fluid media. Regarding in CHL-loaded MPs, the findings revealed in PBS media that $5.13 \pm 0.72$%, was the percent CHL determined after 24 h in its media. To evaluate drug release patterns and show that the release profile was solely controlled by bacteria, we also looked at fluid imitating illness (TSB) without bacteria. The findings revealed the percentage of CHL released in TSB media was $5.34 \pm 1.06$ after 24 h. It was discovered that both media had lower CHL levels compared to pure chloramphenicol. This was because there was no bacterial enzyme stimulus to lyse the polycaprolactone polymer, which would have allowed the medication to stay stable in the microparticle polymer matrix. According to the statistical analysis, there was no statistically significant difference between the release profiles of CHL-loaded MPs and chloramphenicol when compared to PBS and


https://doi.org/10.1021/acsami.2c16857
ACS Appl. Mater. Interfaces XXXX, XXX, XXX−XXX

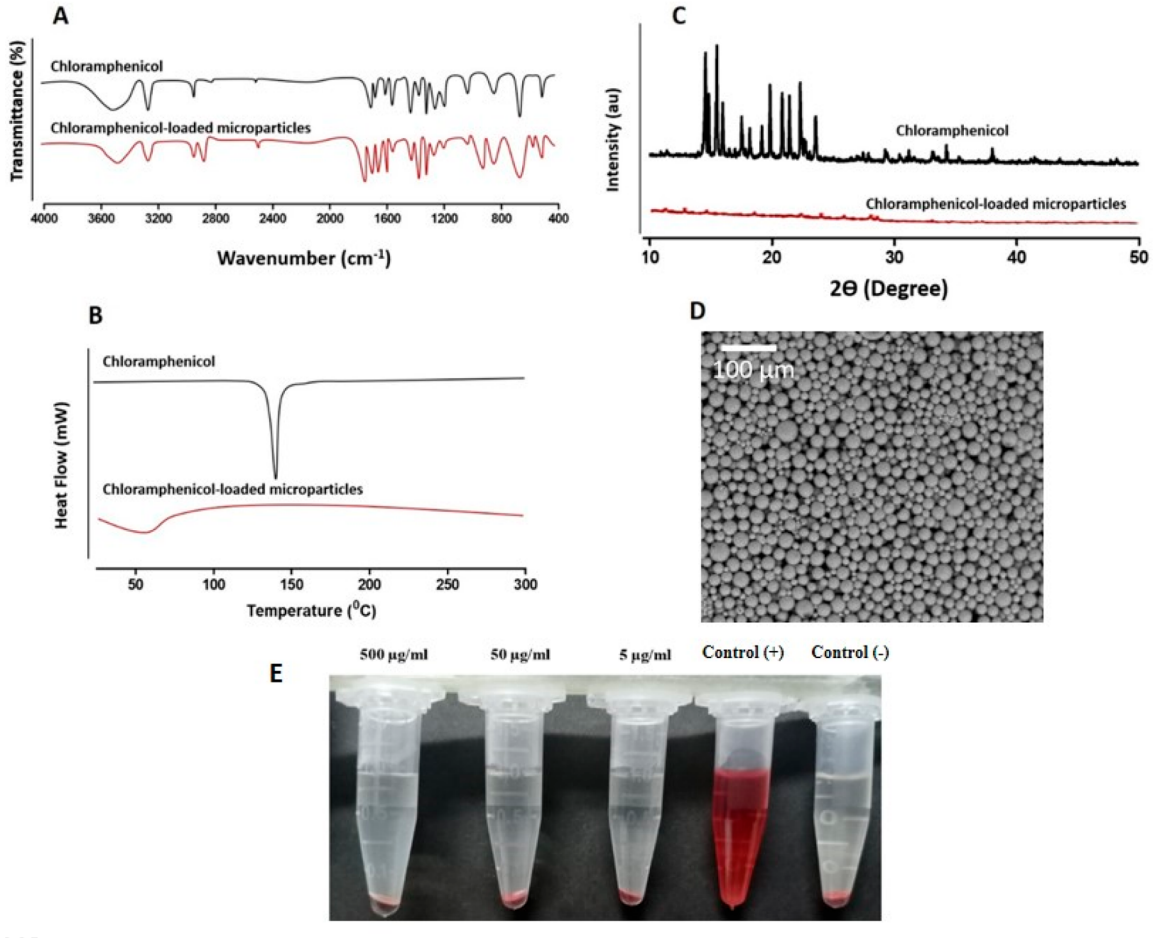


**Figure 5.** (A) FTIR spectra of CHL and CHL-loaded MPs. (B) DSC thermogram of CHL and CHL-loaded MPs. (C) X-ray diffractogram of CHL and CHL-loaded MPs. (D) SEM images of CHL-loaded MPs (the white scale bar represents a length of 100 $\mu$m in each case). (E) Determination of hemolytic activity of CHL-loaded MPs at concentration ranges of 5 $\mu$g/mL, 50 $\mu$g/mL, and 500 $\mu$g/mL by comparing the color of the serum and plasma with that of positive and negative controls.

TSB media ($p > 0.05$). This demonstrated that release in the bacterial responsive microparticle system was unaffected by the environment devoid of bacteria.

Regarding the *in vitro* release profile of CHL-loaded MPs on TSB medium with presence of bacteria, the percentage of CHL determined after 24 h in CHL-loaded MPs was 110.66 ± 13.04%. The TSB Media that presence of bacteria demonstrated higher drug release. This is due to bacteria culture in media producing lipase enzymes that were used to lyse the MPs matrix and detect chloramphenicol concentrations in the medium.[46]

The statistical analysis revealed that the bacterial TSB media with PBS and the absence of bacteria had noticeably different release profiles. Figure 6 shows the levels of pure CHL in all test medium reached close to 100% after 3 h of administration. The MPs preparation in media that contained bacteria reached up to 100% after 8 h. It is suggested that microparticle production can sustain the release of CHL, hence extending the period of exposure to bacteria. This is a good strategy for the administration of antibiotics.

The increased release of CHL from MPs in the presence of bacteria is due to the fact that the presence of bacteria can produce enzymes specifically to accelerate degraded PCL matrix. This is supported by the fact that no drug release was observed when the MPs were suspended in the sterile culture media. This outcome aligned with that of Wu et al., who found that the inclusion of an enzyme stimulate PCL degradation by a factor of 1000 fold in comparison to degradation in an aqueous medium alone.[47] The suggested technique has the potential for selective delivery at infection sites, as seen by the significant difference in CHL release depending on the presence and absence of the bacterium. These findings therefore show that loading CHL into a flexible MPs system can prevent release at nonspecific locations.

To explain the CHL release profile of CHL-loaded MPs, we subsequently fitted the results from the *in vitro* release investigations on bacterial growth medium to five mathematical models. Table 4 displays the findings of the CHL-loaded MPs and CHL release kinetics investigation.

According to *in vitro* release tests, CHL-loaded MPs and pure chloramphenicol matched the kinetic models proposed by zero order (ZO). The prospective use of ZO drug delivery systems may make it possible to accurately control release kinetics and extend therapeutic drug concentration windows. As a result, these systems can increase therapeutic effectiveness, reduce adverse effects, and decrease administration frequency, all of which can lead to improved patient compliance and disease management.[48] This approach has been chosen to characterize drug removal from the polymeric model dependent on polymer response with stimulus bacteria and dispersion of MPs drugs.


https://doi.org/10.1021/acsami.2c16857
ACS Appl. Mater. Interfaces XXXX, XXX, XXX−XXX

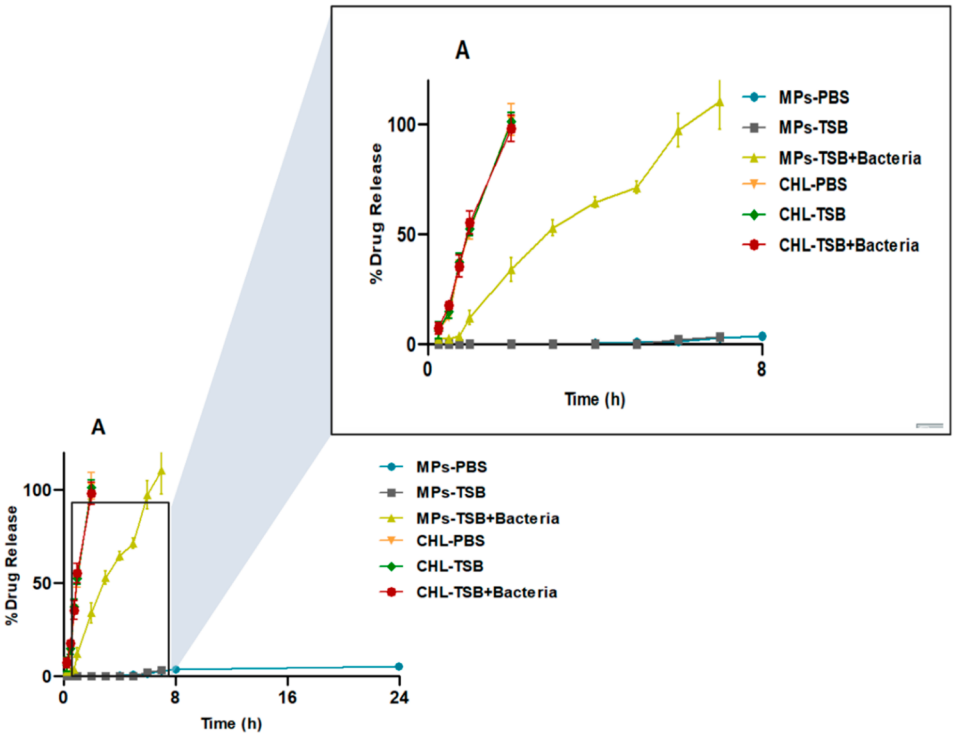


**Figure 6.** *In vitro* release profile of CHL-loaded MPs and CHL in several media (mean ± SD, $n = 3$).

**Table 4. Representative Kinetic Model of Drug Release MP-CHL**

| | kinetic model | | | | |
|---|---|---|---|---|---|
| formulation | zero order | first order | Higuchi | Korsmeyer–Peppas | Hixson–Crowell |
| CHL | 0.9851 | 0.8334 | 0.8167 | 0.9391 | 0.9226 |
| CHL-loaded MPs | 0.9902 | 0.6800 | 0.7658 | 0.9132 | 0.7716 |

**3.7. *In Vitro* Antibacterial Assays.** *3.7.1. MIC and MBC.* Furthermore, investigation was conducted into the antibacterial activity of formulations containing free CHL and CHL-loaded MPs. Table 5 describes the comparisons of MIC and MBC

**Table 5. MIC of Free CHL and CHL-Loaded MPs**

| | concentration (ppm) | | | | | | |
|---|---|---|---|---|---|---|---|
| antimicrobial properties | 200 | 100 | 50 | 25 | 12.5 | 6.25 | 3.125 |
| CHL | (−) | (−) | (−) | (−) | (−) | (+) | (+) |
| CHL-loaded MPs | (−) | (−) | (−) | (−) | (−) | (+) | (+) |

values between the CHL solution and their MP formulations. The MIC value for CHL-loaded MPs against SA ATCC 25923 was 12.5 μg/mL, which same that of free CHL (12.5 μg/mL); see Table 4. The MBC value of CHL-loaded MPs (25 μg/mL) was equal to the MBC of free CHL (25 μg/mL).

Based on the findings, CHL and CHL-loaded MPs may be classified as an intermediate category for the inhibition of SA strains. According to the clinical and laboratory standards institute criteria, MIC ≤ 8 μg/mL was considered susceptible, ≤ 16 μg/mL was considered intermediate, and ≥32 μg/mL was considered resistant.[49]

All MBC values in this investigation were greater than MIC values, demonstrating that higher CHL concentrations were necessary to inhibit the bacterial cultures. When comparing the ratio of MBC to MIC, it was discovered that this ratio was always 4. Bacteriostatic is indicated by a ratio of less than 4 and bactericidal by a ratio of 4.[50] As a result, our research suggested that CHL and CHL-loaded MPs both have bactericidal properties.

**3.8. *In Vivo* Investigation on a Drosophila Larval Infection Model.** The evaluation of antimicrobial activity of CHL-loaded MPs against SA ATCC 25923 was carried out using Drosophila larvae as the infection model. Drosophila larvae have recently been used in the infection experiment to demonstrate the virulence of three clinical strains of SA.[30] From previous research, it is evident that the larval model of infection is easy-to-use and can serve as a suitable host for SA infection and thus is beneficial for use as a rapid in vivo screening platform. In our investigation, we employed the immunodeficient line. Psh and ModSP, a mutant line lacking two important components in the Toll pathway. The absence of these components thus prevents the production of AMPs, which is necessary for the activation of humoral innate immunity in response to SA infection in Drosophila.[51,52] This results in a condition that resembles immunodeficiency, facilitating the easy preparation of an infection model. Such mutant flies have been demonstrated to succumb to pathogens faster than their wild-type counterparts.[53,54] Through this model of infection, we can rule out the role of Toll-mediated innate immunity responses in Drosophila that play a major role in SA infection, thereby confirming the antibacterial effect of the drug candidates.

For the preliminary investigation, we tested dyed microparticles to examine if the microparticles created could be delivered orally to a Drosophila larval model (see Figure 7D). If the MPs entered orally, they were visible on the larvae abdomen. Based on the findings, the MPs were successfully visible on the larva abdomen under a microscope after concomitant oral administration.


https://doi.org/10.1021/acsami.2c16857
ACS Appl. Mater. Interfaces XXXX, XXX, XXX−XXX

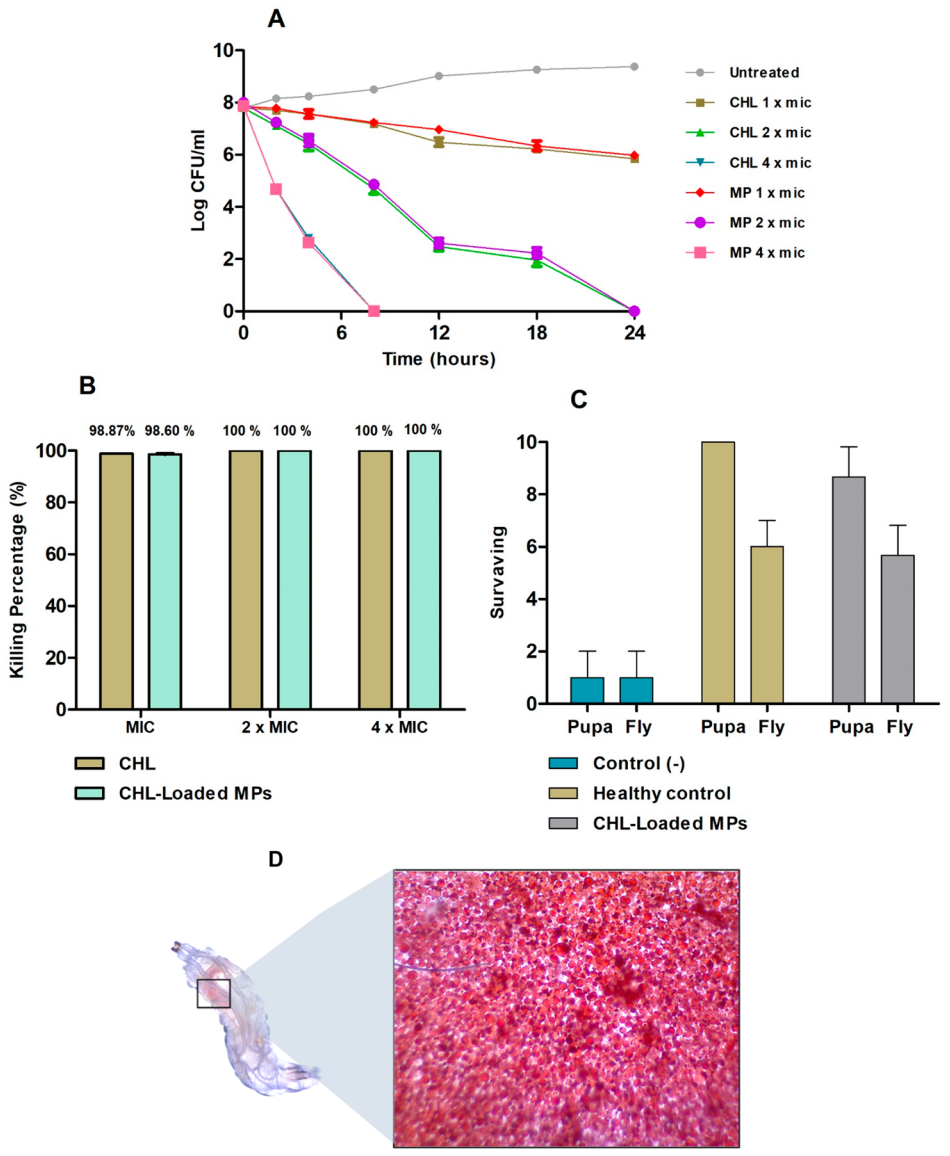


**Figure 7.** (A) Time kill assay of CHL and CHL-loaded MPs against SA (means ± SD, $n = 3$). (B) Anti-infection activity in 96 well microtiter plate of CHL and CHL-loaded MPs against SA (means ± SD, $n = 3$). (C) Survival of psh[1];;modSP[KO] *Drosophila melanogaster* larvae upon 30 min of oral infection with SA in terms of pupae and adult flies' parameters. (D) Trial study to observe coloring microparticles after concomitant oral administration in a Drosophila larva model.

Infection parameters were assessed by counting the number of pupae that have successfully formed, and how many pupae succeeded in becoming adult flies. If the infected larvae grow to form pupae, there are two chances that a pupa will not develop into an adult fly, according to our hypothesis. The first possibility is that an increase bacterial infection burden causes larvae to die during the pupa stage. Another possibility is that the infection causes the energy generated to focus on infection recovery, leaving insufficient energy for the pupa to become an adult fly. Based on Figure 7C, infected larvae without treatment showed larval death; only a few survived to become pupae and adult flies. According to several studies, the increased mortality rate of the dying host has been connected to bacterial load,[52] since giving CHL-loaded MPs, which was mixed on fly food, increased the survival rate of infected Drosophila larva. Because this finding is not significantly different than in healthy controls ($p > 0.05$), it is tempting to assume that this phenotype was caused by the prevention of the bacterial growth *in vivo* model. According to these results, there are two possible steps of the MP system that could accelerate the killing of bacteria, thereby preventing larvae death. The MPs were initially linked to the infection by the outer layer of PCL. After that, the presence of the bacterial strains lipase destroyed PCL layers, causing the release of CHL from MPs, which then killed the bacteria. This supports earlier researchers' findings that Toll immunodeficient flies were more susceptible to bacterial infection. Additionally, similar outcomes were seen in psh[1];;modSP[KO] mutant flies that lacked cellular innate immunity and have a lower survival rate than healthy controls.[52] This mutant fly might survive longer in the presence of CHL-loaded MPs because it lacks the cellular innate immunity that is known to defend against SA. These findings revealed that the antibacterial activity of CHL-loaded MPs against SA was not based on activation of cellular


https://doi.org/10.1021/acsami.2c16857
ACS Appl. Mater. Interfaces XXXX, XXX, XXX−XXX

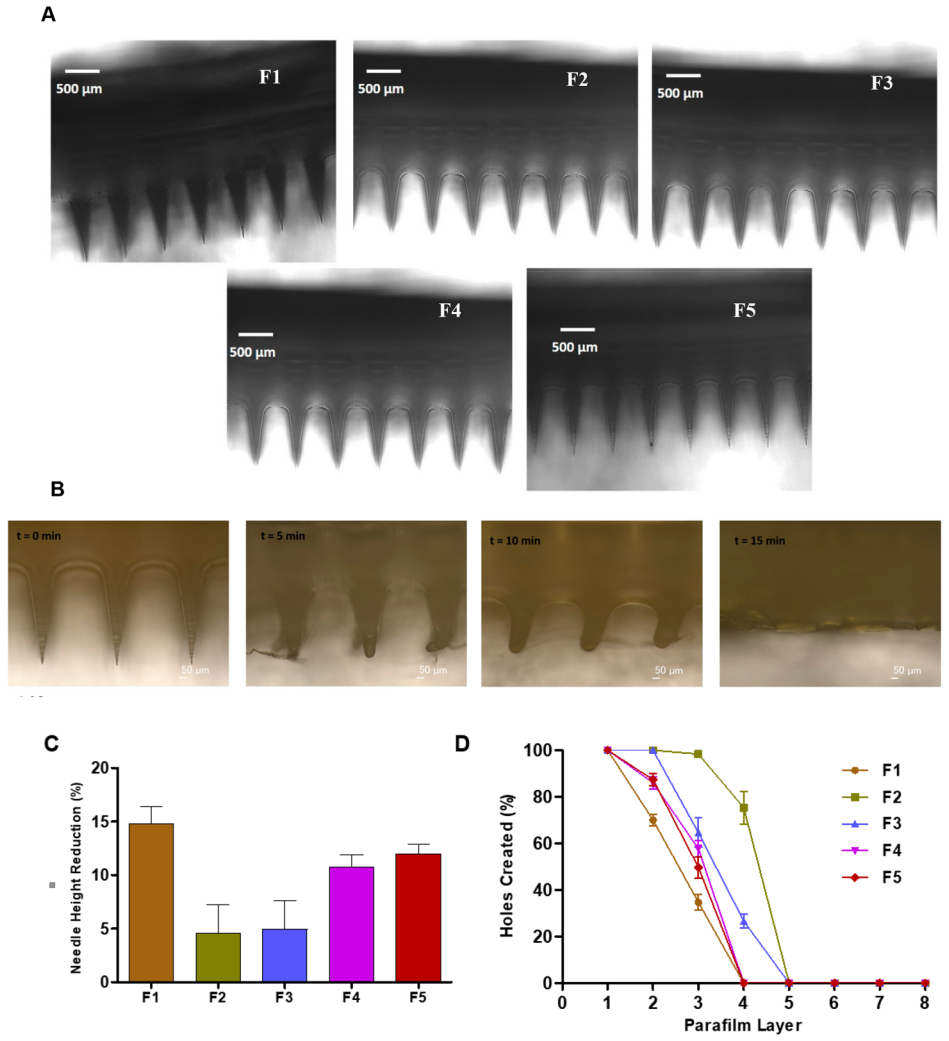


**Figure 8.** (A) Images taken under a light microscope of the MP-containing MN formulations. (B) Morphology of a dissolving microneedle containing CHL-loaded MPs after skin administration. (C) The percentage height reduction of needles on the arrays formulated containing free CHL and CHL-loaded MPs compared to blank MN arrays (means ± SD, $n = 3$). (D) Percentage of holes created in Parafilm layers, using an insertion force of 32N/array for MN formulations containing CHL-loaded MPs (means ± SD, $n = 3$).

immunological responses, but rather by direct interactions between chemicals present in the MPs and bacteria.

**3.9. Fabrication of Two-Layered MNs.** CHL is ineffective for the topical treatment of skin infections due to its hydrophobic chemical components, which limits effective cutaneous penetration. Barriers to effective penetration include thicker skin and the formation of biofilms that inhibit drug penetration to the site of infection. Therefore, the CHL-loaded MPs in this investigation were further formed into MN arrays to enhance the penetration of the antibacterial agents and can responsively disrupt contact with the bacterial infection site. The dissolving MNs were created by combining PVA and PVP, two water-soluble polymers. In our earlier research, dissolving MNs with adequate mechanical characteristics could not be created using a single polymer.[23,25] In contrast, the C═O groups of PVP and the −OH groups of PVA interact to create a hydrogen bond, increasing the mechanical strength of MNs.[25] Figure 8A illustrates the morphologies of MNs seen under a light microscope, demonstrating that all DMN formulations created sharp needles. In this investigation, two-layered MN formulations with various polymer concentrations were created to find the best mechanical properties.

**3.10. Evaluation of Mechanical and Insertion Properties of Dissolving MNs.** The mechanical toughness of the MN arrays was assessed to ensure that MN arrays were strong enough to resist compression. The ability of MNs to be inserted into the skin is important since the needle must be able to break through the stratum corneum in order to deliver the substance drug into the normal skin layers.[55] In this study, we measured how much the MN needle height was reduced following 32 N/MN array, which is equivalent to the pressure of compression by a human hand. A calculation was made to determine the mechanical strength. The mechanical characteristics of each formulation are shown in Figure 8C as a percentage reduction in MNs and a comparison of the height of the needle before pressure force was applied. For MNs-F1, MNs-F2, MNs-F3, MNs-F4, and MNs-F5, the decreases in MN height were determined to be 14.82 ± 1.55%, 4.56 ± 2.66%, 4.96 ± 2.66%, 10.73 ± 1.17%, and 11.97 ± 0.89%, respectively. As a result, the mechanical characteristics of the dissolving MN arrays were unaffected by the formulation of CHL-loaded MPs. Despite the


https://doi.org/10.1021/acsami.2c16857
ACS Appl. Mater. Interfaces XXXX, XXX, XXX−XXX

**Table 6. Particle Size, PDI, Zeta Potential, EE, and DL of Formulations of CHL-Loaded MPs in MN Formulation (mean ± SD, $n$ = 3)**

| characteristics | day 0 | day 3 | day 7 | day 10 |
|---|---|---|---|---|
| particle size ($\mu$m) | 25.43 ± 1.32 | 24.65 ± 1.54 | 25.65 ± 1.31 | 25.87 ± 1.45 |
| PDI | 0.054 ± 0.003 | 0.043 ± 0.004 | 0.051 ± 0.005 | 0.049 ± 0.004 |
| zeta potential (mV) | −7.19 ± 0.44 | −7.09 ± 0.36 | −7.11 ± 0.52 | −7.05 ± 0.43 |
| EE (%) | 39.69 ± 2.76 | 39.54 ± 2.65 | 38.56 ± 3.01 | 38.44 ± 2.41 |
| DL (%) | 18.43 ± 1.34 | 18.31 ± 1.17 | 18.16 ± 1.37 | 18.14 ± 1.29 |

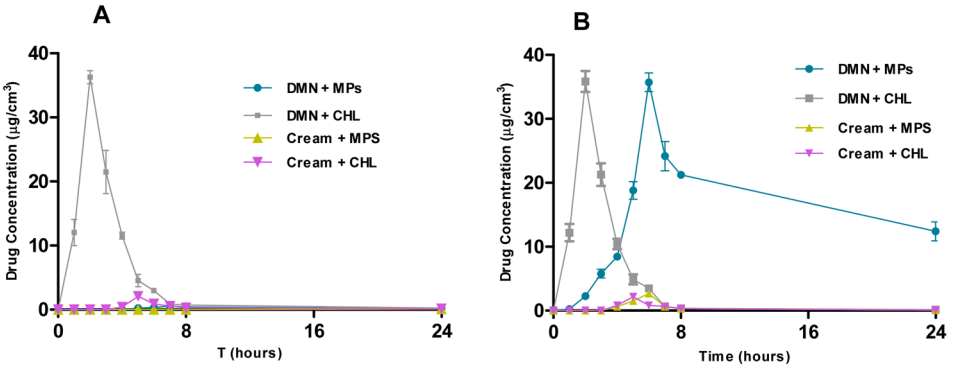


**Figure 9.** (a) *Ex vivo* concentrations and time profiles of CHL following the application of DMN-MPs, DMN-CHL, cream-MPs, and cream-CHL in noninfected rat skin, as well as (b) *ex vivo* infection models formed by SA (means ± SD, $n$ = 3).

**Table 7. List of the Dermatokinetic Characteristics of Chloramphenicol in Uninfected Rat Skin As Well As Ex Infection Models Created by SA after the Administration of DMN-MPs, DMN-CHL, Cream-MPs, and Cream-CHL (means SD, $n$ = 3)**

| condition | formulation | $C_{max}$ ($\mu$g/cm$^3$) | $T_{max}$ (h) | $T_{1/2}$(h) | AUC 0-t ($\mu$g/cm$^3$ h) | AUC 0-inf_obs ($\mu$g/cm$^3$ h) | MRT (h) |
|---|---|---|---|---|---|---|---|
| normal skin | DMN-MPs | 0.58 ± 0.11 | 6.33 ± 1.15 | 12.30 ± 8.87 | 6.33 ± 1.20 | 10.09 ± 5.40 | 21.06 ± 14.16 |
| | DMN-CHL | 36.27 ± 1.01 | 2.00 ± 0.00 | 4.89 ± 1.35 | 97.81 ± 2.62 | 99.41 ± 3.44 | 3.87 ± 0.76 |
| | cream-MPs | 0.12 ± 0.07 | 24.00 ± 0.00 | N/A | 1.41 ± 0.83 | N/A | N/A |
| | cream-CHL | 2.08 ± 0.47 | 5.00 ± 0.00 | 7.02 ± 2.14 | 7.99 ± 1.50 | 9.59 ± 1.62 | 13.06 ± 4.91 |
| infected skin By SA | DMN-MPs | 35.73 ± 1.43 | 6.00 ± 0.00 | 19.79 ± 6.03 | 375.38 ± 9.57 | 737.55 ± 160.00 | 31.67 ± 8.62 |
| | DMN-CHL | 35.86 ± 1.63 | 2.00 ± 0.00 | 5.76 ± 3.46 | 92.95 ± 1.93 | 94.06 ± 2.48 | 3.48 ± 0.33 |
| | cream-MPs | 2.67 ± 0.29 | 6.00 ± 0.00 | 6.39 ± 2.05 | 9.58 ± 1.24 | 10.52 ± 1.77 | 9.81 ± 1.94 |
| | cream-CHL | 2.19 ± 0.46 | 5.00 ± 0.00 | 6.39 ± 2.67 | 8.68 ± 2.98 | 9.64 ± 3.43 | 10.03 ± 2.44 |

fact that F4 and F5 had larger percentages of height losses than F2 and F3, several studies have indicated that DMN formulations with a height decrease percentage of about 25% were acceptable.[56]

Eight layers of Parafilm were used as a skin stimulant for the insertion qualities force. This model has been certified to mimic human skin for MN insertion investigations.[55] The study's results are shown in Figure 8D. The formulation of the MN regarding different polymer concentrations (PVA and PVP), as mentioned previously, had no effect on any of the MNs' insertion qualities ($p$ > 0.05), similar to how it had no effect on the mechanical properties. Four layers of Parafilm were able to be penetrated by the MN arrays. The typical thickness of each layer of Parafilm is 126 $\mu$m. Thus, DMNs were placed up to a height of 378 $\mu$m. F1, F4, and F5 produced holes in the third layer that were responsible for 34.66 ± 5.85%, 57.66 ± 6.11%, and 49.66 ± 8.02%, respectively, of the total holes. F2 and F3 produced holes in four layers and were respectively responsible for 75.33 ± 12.01% and 26.66 ± 5.13%, of the total holes. As a result, F2 was chosen for further testing since it had a good penetration layer and holes created compared to other formulas.

To estimate how long it would take for the needles to dissolve in the skin after administration, we examined dissolution experiments of MN formulations incorporating drug-loaded MPs. According to Figure 8B, breakdown of MNs while in the skin occurred after 15 min, with needle disintegration and a drop in height being apparent after 5 min. This showed that the formulation met acceptable criteria for MN formulations.

**3.11. Calculation of Drug Content Localized to the Needles.** Upon drying the MN arrays, it was found that each one contained 70.58 $\mu$g of CHL, with a percent recovery of 98.09 ± 1.82%. The dose of CHL in one MN array in the succeeding trials was thus reflected by these medication quantities.

**3.12. Stability Test of MP-CHL Loaded into Dissolving Microneedle.** The capacity of the formulations to preserve the MPs' stability, especially their sizes, PDIs, entrapment efficiency, drug loading, and zeta potentials, is one of the essential criteria in the formulation of MPs into dissolving MNs. Table 6 shows the MP characteristics in the MNs formulations. These results imply that the particle size, EE%, DL%, and zeta potential of CHL-loaded MPs were not significantly ($p$ > 0.05) affected by the inclusion of MPs into MNs arrays. Regarding the PDI value, it increased after being added to MNs but still produced a PDIs below 0.05, indicating that the formulations are still homogeneous and monodisperse.

**3.13. *Ex Vivo* Dermatokinetic Studies.** The main goal in this investigation was to determine the dermatokinetical profile


https://doi.org/10.1021/acsami.2c16857
ACS Appl. Mater. Interfaces XXXX, XXX, XXX−XXX

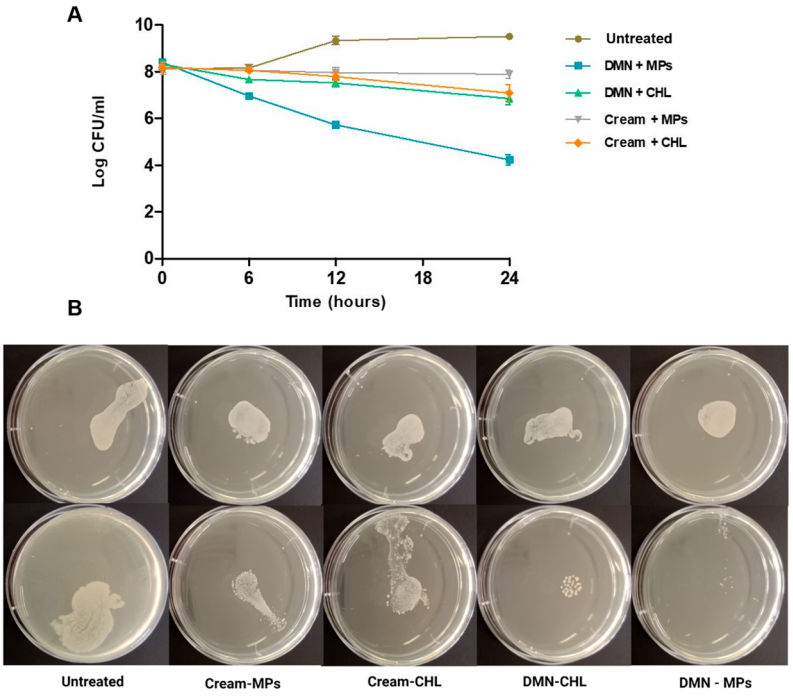


**Figure 10.** (A) Bacterial viability (log CFU/mL) on in *ex vivo* infection models formed by SA following the application of dissolving MNs-CHL, MNs-MPs, cream-CHL, and cream-MPs (means ± SD, $n = 3$). (B) Images of culture plates showing the *ex vivo* removal of SA infection from wounds on rat skin at interval times of 0 (above) and 24 h (below).

of CHL-loaded MPs in skin layers, where SA colonizes, infects, and produces wound skin infection. In order to do this, a dermatokinetic analysis was created and carried out to examine the CHL release kinetics from MPs following MN application. This study employed normal skin and infected model on rat skin tissue to prove that the presence of a bacterial infection is the only impact on the release of chloramphenicol in the skin, and chloramphenicol secreted by MPs was assessed. This was done in order to determine how much CHL was retained in the skin by vortexing the skin samples with water at each interval. Our findings demonstrated that this method would extract only CHL produced by MPs because no CHL was discovered in the MP dispersion's supernatant after sample vortexing.

The dermatokinetic profile of our method in this investigation was compared to MNs containing CHL-loaded MPs (MNs-CHL MPs) and without MPs formulation (MNs-CHL). To compare their effectiveness with the previously stated methods, we also evaluated the dermatokinetic properties of a conventional cream containing CHL (cream-CHL) and cream containing CHL-loaded MPs (cream-CHL MPs). Figure 9a, b shows the concentration of CHL released with another approach delivery system in the skin vs application time following its application. The dermatokinetic parameters of CHLs, including $C_{max}$, $T_{max}$, $T_{1/2}$, AUC, and MRT, were also calculated as shown in Table 7. This result demonstrated, in the absence of bacterial growth in normal skin, MNs-CHL MPs produced CHL concentrations significantly lower than MNs-CHL ($p < 0.05$). This phenomenon also occurs in the application system for conventional cream preparations. Due to the justifications given for the $C_{max}$ results, the $T_{max}$ values of CHL from MNs-CHL MPs was also discovered to be significantly lower ($p < 0.05$) than those from the other formulations in normal skin. This suggested that the nonspecific release (normal skin test) of CHL may be prevented by incorporating CHL into MPs. The level of $C_{max}$ of CHL in conventional cream preparations was significantly lower than in MN preparations ($p < 0.05$). This was due to the hydrophobic chemical components of CHL and CHL-loaded MPs, which limit effective cutaneous penetration. This is a proof of concept that the application of the MN system can increase the concentration drug penetration for dermal drug administration.

Regarding *ex vivo* infection models using SA, the release of chloramphenicol from MNs-MPs was significantly enhanced ($p < 0.05$) compared to that from MNs-CHL. According to the findings of this study, CHL encapsulation in the PCL matrix may boost CHL concentration through two separate methods. The MPs' initial adhesion to the colony infection was made easier by the PCL outer layer. After that, the environment was exposed to bacterial strains whose lipase broke down PCL layers, releasing CHL from MPs.

Regarding AUC, it was discovered that the AUC values of CHL from MNs-MPs in *ex vivo* infection models were considerably greater ($p > 0.05$) than those of other formulations, demonstrating the improved *ex vivo* skin bioavailability of our strategy. To assess retention duration in the skin, we examined the MRT parameter, which shows how long drug molecules stay in skin tissue. It was discovered that the MRT values of CHL from DMN-MPs were significantly higher ($p < 0.05$) than those of MNs-CHL, cream-MPs, and cream-CHL, demonstrating a longer retention period in the skin. Because of the enhanced MRT, a shorter application period for CHL in the treatment of skin infections may be feasible. As a result, it could influence patients to adopt this approach. Our results suggest that chloramphenicol may be effectively transferred into an *ex vivo* infection model via a combination of responsive MPs and MNs.

**3.14. Anti-infection Activity in *Ex Vivo* Model of Infection on Rat Skin.** The reduction of bacterial bioburdens in *ex vivo* infection models made of SA was examined by


https://doi.org/10.1021/acsami.2c16857
ACS Appl. Mater. Interfaces XXXX, XXX, XXX−XXX

measuring the viable cell counts to evaluate the effectiveness of this strategy. In an *ex vivo* rat skin wound model, postinfection CFU counts revealed a significant decrease in microbial load in all various treated wounds compared to untreated wounds. Figure 10A, B displays the study's findings. Regarding conventional cream preparations, only around 90.77 ± 6.46% of the bacterial bioburden was reduced after 24 h, while when MPs-CHL was made into cream, it resulted in a 58.88 ± 8.38% decrease in bacterial bioburden, resulting in the lowest anti-infection performance in *ex vivo* infection models

Regarding DMN preparation, CHLs were applied to both bacterial *ex vivo* infection models, and the results showed a 96.38 ± 1.27% decrease in bacterial bioburden after 24 h of treatment. DMNs containing MPs-CHL showed a 99.99 ± 0.01% decrease. Although the $C_{max}$ of MN-free CHL was greater than the MBC of CHL to bacterial strain, the retention period of CHL after application was less than the time required by CHL to totally kill the bacteria. Consequently, only around 96.38% of the bacterial loads of the strain decreased after the administration of MN-free CHL. This suggested that DMNs could enhance the effectiveness of CHL as anti-infection agents. A number of studies have demonstrated that adding antibacterial drugs to MNs increased their antibacterial activity.[57,20,33,58] Essentially, the adoption of this strategy was able to completely remove the SA since DMN-MPs had the optimum *ex vivo* skin bioavailability in the dermatokinetic testing. Consequently, there were two key advantages of administering CHL that were loaded with PCL-MPs and delivered via DMNs.

The dermatokinetic profiles in this investigation show that manufacturing CHL into MPs could be improved and controlled using this method as opposed to conventional cream formulation. This method may increase the effectiveness of CHL in *ex vivo* infection models in rat skin generated by SA.

The study's hypothesis that responsive MPs containing CHL may be successfully delivered into the skin via dissolving MNs and can then demonstrate their antibacterial action at the site of infection has been supported by the study's encouraging preliminary findings. The ability for site-selective delivery and long retention time in the area of infection in the skin, which may potentially increase the efficacy of antibacterial therapy for burns and chronic wounds, are the key advantages of the selective delivery system we have developed here compared to conventional cream dosage form. DMNs might therefore be employed to deliver antimicrobial drugs topically to wounds, and their combination with certain MPs could be a feasible substitute for existing antimicrobial treatment strategies.

## 4. CONCLUSION

To improve the antibacterial capability of CHL, specifically for the treatment of cellulitis, this study explored the novel combination strategy of bacterially sensitive MPs with dissolving MN arrays. The MPs had a diameter of about 24.33 $\mu$m and were spherical in form. Additionally, the presence of bacterial cultures had a significant impact on the release of CHL from the MPs, demonstrating the effectiveness of this approach for targeted delivery. The evaluation of the antibacterial activity of MPs *in vitro* and *in vivo* on the mutant Drosophila larval infection model was carried out. This result demonstrates antibacterial properties of CHL; after being made into a bacterial responsive microparticle system, its efficacy did not decrease. It is significant that adding these MPs to MN arrays made from PVP and PVA combined with these MPs gave rise to MNs with adequate mechanical characteristics and insertion capabilities. In infection tissue models in full-thickness rat skin, dermatokinetic experiments showed that the MNs improved the ability of MPs to penetrate bacteria when compared to a needle-free patch. Finally, the combined method of microparticle responsive bacteria with dissolving MNs demonstrated a proof of principle for successful anti-infection action in *ex vivo* infection models, as evidenced by a reduction of bacterial bioburden up to 99.99%. However, more thorough research is required, including toxicity tests and in vivo pharmacodynamic research using appropriate animal infection models. Acceptance and usability studies should be carried out to confirm the work's full potential before integrating this delivery method into clinical practice and patient treatment.

## AUTHOR INFORMATION


### Corresponding Author

**Andi Dian Permana** − *Department of Pharmaceutics, Faculty of Pharmacy, Hasanuddin University, Makassar 90245, Indonesia;* orcid.org/0000-0003-2168-1688; Email: andi.dian.permana@farmasi.unhas.ac.id

### Authors

**Mukarram Mudjahid** − *Department of Pharmaceutics, Faculty of Pharmacy, Hasanuddin University, Makassar 90245, Indonesia*

**Firzan Nainu** − *Department of Pharmacology and Toxicology, Faculty of Pharmacy, Universitas Hasanuddin, Makassar 90245, Indonesia*

**Rifka Nurul Utami** − *Department of Pharmaceutics, Faculty of Pharmacy, Hasanuddin University, Makassar 90245, Indonesia*

**Anwar Sam** − *Department of Pharmaceutics, Faculty of Pharmacy, Hasanuddin University, Makassar 90245, Indonesia*

**Ardiyah Nurul Fitri Marzaman** − *Department of Pharmaceutics, Faculty of Pharmacy, Hasanuddin University, Makassar 90245, Indonesia*

**Tri Puspita Roska** − *Department of Pharmaceutics, Faculty of Pharmacy, Hasanuddin University, Makassar 90245, Indonesia*

**Rangga Meidianto Asri** − *Department of Pharmaceutics, Faculty of Pharmacy, Hasanuddin University, Makassar 90245, Indonesia*

**Achmad Himawan** − *Department of Pharmaceutics, Faculty of Pharmacy, Hasanuddin University, Makassar 90245, Indonesia;* orcid.org/0000-0002-2017-3406

**Ryan F. Donnelly** − *School of Pharmacy, Queen's University Belfast, Medical Biology Centre, Belfast BT9 7BL, United Kingdom;* orcid.org/0000-0002-0766-4147

Complete contact information is available at: https://pubs.acs.org/10.1021/acsami.2c16857


### Author Contributions

The manuscript was written through contributions of all authors.

### Notes

The authors declare the following competing financial interest(s): Ryan Donnelly is an inventor of patents that have been licensed to companies developing microneedle-based products and is a paid advisor to companies developing microneedle-based products. The resulting potential conflict of interest has been disclosed and is managed by Queen's University Belfast. The companies had no role in the design of



https://doi.org/10.1021/acsami.2c16857
ACS Appl. Mater. Interfaces XXXX, XXX, XXX−XXX

the present studies, in the collection, analyses, or interpretation of the data, in the writing of the manuscript, or in the decision to publish the work.

## ■ ACKNOWLEDGMENTS

Mukarram Mudjahid is thankful for the scholarship provided by German Academic Exchange Service (Deutscher Akademischer Austausch Dienst/DAAD). This study was also supported by Penelitian Tesis Magister, Ministry of Education, Culture, Research, and Technology of Republic of Indonesia (090/E5/PG.02.00/PT/2022).

## ■ REFERENCES

(1) Clinton, A.; Carter, T. Chronic Wound Biofilms: Pathogenesis and Potential Therapies. *Lab Med.* **2015**, *46* (4), 277−284.
(2) Rondas, A. A. L. M.; Schols, J. M. G. A.; Stobberingh, E. E.; Halfens, R. J. G. Prevalence of Chronic Wounds and Structural Quality Indicators of Chronic Wound Care in Dutch Nursing Homes. *Int. Wound J.* **2015**, *12* (6), 630−635.
(3) El-Mohri, H.; Wu, Y.; Mohanty, S.; Ghosh, G. Impact of Matrix Stiffness on Fibroblast Function. *Mater. Sci. Eng., C* **2017**, *74*, 146−151.
(4) Raff, A. B.; Kroshinsky, D. Cellulitis A Review. *Jama* **2016**, *316* (3), 325−337.
(5) Rrapi, R.; Chand, S.; Kroshinsky, D. Cellulitis: A Review of Pathogenesis, Diagnosis, and Management. *Med. Clin. North Am.* **2021**, *105* (4), 723−735.
(6) Andersen, C. A.; McLeod, K.; Steffan, R. Diagnosis and Treatment of the Invasive Extension of Bacteria (Cellulitis) from Chronic Wounds Utilising Point-of-Care Fluorescence Imaging. *Int. Wound J.* **2022**, *19*, 996−1008.
(7) Bou Haidar, N.; Marais, S.; Dé, E.; Schaumann, A.; Barreau, M.; Feuilloley, M. G. J.; Duncan, A. C. Chronic Wound Healing: A Specific Antibiofilm Protein-Asymmetric Release System. *Mater. Sci. Eng., C* **2020**, *106*, 110130.
(8) Mihai, M. M.; Preda, M.; Lungu, I.; Gestal, M. C.; Popa, M. I.; Holban, A. M. Nanocoatings for Chronic Wound Repair—Modulation of Microbial Colonization and Biofilm Formation. *Int. J. Mol. Sci.* **2018**, *19* (4), 1179.
(9) Gemeinder, J. L. P.; Barros, N. R. d.; Pegorin, G. S.; Singulani, J. d. L.; Borges, F. A.; Arco, M. C. G. D.; Giannini, M. J. S. M.; Almeida, A. M. F.; Salvador, S. L. d. S.; Herculano, R. D. Gentamicin Encapsulated within a Biopolymer for the Treatment of Staphylococcus Aureus and Escherichia Coli Infected Skin Ulcers. *J. Biomater. Sci. Polym. Ed.* **2021**, *32* (1), 93−111.
(10) Sartini, S.; Permana, A. D.; Mitra, S.; Tareq, A. M.; Salim, E.; Ahmad, I.; Harapan, H.; Emran, T. Bin; Nainu, F. Current State and Promising Opportunities on Pharmaceutical Approaches in the Treatment of Polymicrobial Diseases. *Pathogens* **2021**, *10* (2), 245.
(11) Kotoky, J.; Kandimalla, R.; Kalita, S.; Devi, B.; Sharma, K. K.; Sharma, A.; Kalita, K.; Ch Kataki, A. Chloramphenicol Encapsulated in Poly-ε-Caprolactone-Pluronic Composite: Nanoparticles for Treatment of MRSA-Infected Burn Wounds. *Int. J. Nanomedicine* **2015**, *10*, 2971−2984.
(12) Abdollahi, M.; Mostafalou, S.Chloramphenicol. *Encyclopedia of Toxicology*, third ed.; Elsevier, 2014; Vol. *1*, pp 837−840.
(13) Shukla, P.; Bansode, F. W.; Singh, R. K. Chloramphenicol Toxicity : A Review. *J. Med. Med. Sci.* **2011**, *2* (13), 1313−1316.
(14) Allen, T. M.; Cullis, P. R. Drug Delivery Systems: Entering the Mainstream. *Science (80-.).* **2004**, *303* (5665), 1818−1822.
(15) Chatterjee, S.; Chi-leung Hui, P. Review of Stimuli-Responsive Polymers in Drug Delivery and Textile Application. *Molecules* **2019**, *24* (14), 2547.
(16) Ayaz, P.; Xu, B.; Zhang, X.; Wang, J.; Yu, D.; Wu, J. A PH and Hyaluronidase Dual-Responsive Multilayer-Based Drug Delivery System for Resisting Bacterial Infection. *Appl. Surf. Sci.* **2020**, *527*, 146806.
(17) Xiong, M. H.; Bao, Y.; Yang, X. Z.; Wang, Y. C.; Sun, B.; Wang, J. Lipase-Sensitive Polymeric Triple-Layered Nanogel for "on-Demand" Drug Delivery. *J. Am. Chem. Soc.* **2012**, *134* (9), 4355−4362.
(18) Bettencourt, A.; Ferreira, I.; Goncalves, L.; Kasper, S.; Bertrand, B.; Kikhney, J.; Moter, A.; Trampuz, A.; Almeida, A. J Activity of Daptomycin- and Vancomycin-Loaded Poly-Epsilon-Caprolactone Microparticles against Mature Staphylococcal Biofilms. *Int. J. Nanomedicine* **2015**, *10*, 4351−4366.
(19) Permana, A. D.; Nainu, F.; Moffatt, K.; Larrañeta, E.; Donnelly, R. F. Recent Advances in Combination of Microneedles and Nanomedicines for Lymphatic Targeted Drug Delivery. *Wiley Interdiscip. Rev. Nanomedicine Nanobiotechnology* **2021**, *13* (3), 1−22.
(20) Permana, A. D.; Anjani, Q. K.; Sartini; Utomo, E.; Volpe-Zanutto, F.; Paredes, A. J.; Evary, Y. M.; Mardikasari, S. A.; Pratama, M. R.; Tuany, I. N.; Donnelly, R. F. Selective Delivery of Silver Nanoparticles for Improved Treatment of Biofilm Skin Infection Using Bacteria-Responsive Microparticles Loaded into Dissolving Microneedles. *Mater. Sci. Eng., C* **2021**, *120*, 111786.
(21) Lengyel, M.; Kállai-Szabó, N.; Antal, V.; Laki, A. J.; Antal, I. Microparticles, Microspheres, and Microcapsules for Advanced Drug Delivery. *Sci. Pharm.* **2019**, *87* (3), 20.
(22) Kalita, S.; Devi, B.; Kandimalla, R.; Sharma, K. K.; Sharma, A.; Kalita, K.; Kataki, A. C.; Kotoky, J. Chloramphenicol Encapsulated in Poly-ε-Caprolactone−Pluronic Composite Nanoparticles for Treatment of MRSA-Infected Burn Wounds. *Int. J. Nanomed.* **2015**, *10*, 2971−2984.
(23) Permana, A. D.; McCrudden, M. T. C.; Donnelly, R. F. Enhanced Intradermal Delivery of Nanosuspensions of Antifilariasis Drugs Using Dissolving Microneedles: A Proof of Concept Study. *Pharmaceutics* **2019**, *11* (7), 346.
(24) Ita, K. Dissolving Microneedles for Transdermal Drug Delivery: Advances and Challenges. *Biomed. Pharmacother.* **2017**, *93*, 1116−1127.
(25) Permana, A. D.; Tekko, I. A.; McCrudden, M. T. C.; Anjani, Q. K.; Ramadon, D.; McCarthy, H. O.; Donnelly, R. F. Solid Lipid Nanoparticle-Based Dissolving Microneedles: A Promising Intradermal Lymph Targeting Drug Delivery System with Potential for Enhanced Treatment of Lymphatic Filariasis. *J. Controlled Release* **2019**, *316*, 34−52.
(26) Badran, M. M.; Alomrani, A. H.; Harisa, G. I.; Ashour, A. E.; Kumar, A.; Yassin, A. E. Novel Docetaxel Chitosan-Coated PLGA/PCL Nanoparticles with Magnified Cytotoxicity and Bioavailability. *Biomed. Pharmacother.* **2018**, *106* (July), 1461−1468.
(27) Yang, Z. G.; Sun, H. X.; Fang, W. H. Haemolytic Activities and Adjuvant Effect of Astragalus Membranaceus Saponins (AMS) on the Immune Responses to Ovalbumin in Mice. *Vaccine* **2005**, *23* (44), 5196−5203.
(28) Radaelli, M.; da Silva, B. P.; Weidlich, L.; Hoehne, L.; Flach, A.; da Costa, L. A. M. A.; Ethur, E. M. Antimicrobial Activities of Six Essential Oils Commonly Used as Condiments in Brazil against Clostridium Perfringens. *Brazilian J. Microbiol.* **2016**, *47* (2), 424−430.
(29) Chen, H.; Li, L.; Liu, Y.; Wu, M.; Xu, S.; Zhang, G.; Qi, C.; Du, Y.; Wang, M.; Li, J.; Huang, X. In Vitro Activity and Post-Antibiotic Effects of Linezolid in Combination with Fosfomycin against Clinical Isolates of Staphylococcus Aureus. *Infect. Drug Resist.* **2018**, *11*, 2107−2115.
(30) Ramond, E.; Jamet, A.; Ding, X.; Euphrasie, D.; Bouvier, C.; Lallemant, L.; He, X.; Arbibe, L.; Coureuil, M.; Charbit, A. Reactive Oxygen Species-Dependent Innate Immune Mechanisms Control Methicillin-Resistant Staphylococcus Aureus Virulence in the Drosophila Larval Model. *MBio* **2021**, *12* (3), e00276-21.
(31) Zhang, Y.; Huo, M.; Zhou, J.; Xie, S. PKSolver: An Add-in Program for Pharmacokinetic and Pharmacodynamic Data Analysis in Microsoft Excel. *Comput. Methods Programs Biomed.* **2010**, *99* (3), 306−314.
(32) Putri, H. E.; Utami, R. N.; Aliyah; Wahyudin, E.; Oktaviani, W. W.; Mudjahid, M.; Permana, A. D. Dissolving Microneedle Formulation of Ceftriaxone: Effect of Polymer Concentrations on Characterisation and Ex Vivo Permeation Study. *J. Pharm. Innov.* **2021**, No. 0123456789.


https://doi.org/10.1021/acsami.2c16857
*ACS Appl. Mater. Interfaces* XXXX, XXX, XXX−XXX

(33) Permana, A. D.; Paredes, A. J.; Volpe-Zanutto, F.; Anjani, Q. K.; Utomo, E.; Donnelly, R. F. Dissolving Microneedle-Mediated Dermal Delivery of Itraconazole Nanocrystals for Improved Treatment of Cutaneous Candidiasis. *Eur. J. Pharm. Biopharm.* **2020**, *154* (June), 50−61.
(34) González-Vázquez, P.; Larrañeta, E.; McCrudden, M. T. C.; Jarrahian, C.; Rein-Weston, A.; Quintanar-Solares, M.; Zehrung, D.; McCarthy, H.; Courtenay, A. J.; Donnelly, R. F. Transdermal Delivery of Gentamicin Using Dissolving Microneedle Arrays for Potential Treatment of Neonatal Sepsis. *J. Controlled Release* **2017**, *265*, 30−40.
(35) Alhusein, N.; Blagbrough, I. S.; Beeton, M. L.; Bolhuis, A.; De Bank, P. A. Electrospun Zein/PCL Fibrous Matrices Release Tetracycline in a Controlled Manner, Killing Staphylococcus Aureus Both in Biofilms and Ex Vivo on Pig Skin, and Are Compatible with Human Skin Cells. *Pharm. Res.* **2016**, *33* (1), 237−246.
(36) Roche, E. D.; Woodmansey, E. J.; Yang, Q.; Gibson, D. J.; Zhang, H.; Schultz, G. S. Cadexomer Iodine Effectively Reduces Bacterial Biofilm in Porcine Wounds Ex Vivo and in Vivo. *Int. Wound J.* **2019**, *16* (3), 674−683.
(37) Mir, M.; Ishtiaq, S.; Rabia, S.; Khatoon, M.; Zeb, A.; Khan, G. M.; ur Rehman, A.; ud Din, F. Nanotechnology: From In Vivo Imaging System to Controlled Drug Delivery. *Nanoscale Res. Lett.* **2017**, *12*, 500.
(38) Ahmadi, M.; Vahabzadeh, F.; Bonakdarpour, B.; Mofarrah, E.; Mehranian, M. Application of the Central Composite Design and Response Surface Methodology to the Advanced Treatment of Olive Oil Processing Wastewater Using Fenton's Peroxidation. *J. Hazard. Mater.* **2005**, *123* (1−3), 187−195.
(39) Budhian, A.; Siegel, S. J.; Winey, K. I. Haloperidol-Loaded PLGA Nanoparticles: Systematic Study of Particle Size and Drug Content. *Int. J. Pharm.* **2007**, *336* (2), 367−375.
(40) Dubey, N.; Varshney, R.; Shukla, J.; Ganeshpurkar, A.; Hazari, P. P.; Bandopadhaya, G. P.; Mishra, A. K.; Trivedi, P. Synthesis and Evaluation of Biodegradable PCL/PEG Nanoparticles for Neuroendocrine Tumor Targeted Delivery of Somatostatin Analog. *Drug Delivery* **2012**, *19* (3), 132−142.
(41) Shalaby, K. S.; Soliman, M. E.; Casettari, L.; Bonacucina, G.; Cespi, M.; Palmieri, G. F.; Sammour, O. A.; El Shamy, A. A. Determination of Factors Controlling the Particle Size and Entrapment Efficiency of Noscapine in PEG/PLA Nanoparticles Using Artificial Neural Networks. *Int. J. Nanomedicine* **2014**, *9* (1), 4953−4964.
(42) Mahmoudi, M.; Saeidian, H.; Mirjafary, Z.; Mokhtari, J. Preparation and Characterization of Memantine Loaded Polycaprolactone Nanocapsules for Alzheimer's Disease. *J. Porous Mater.* **2021**, *28* (1), 205−212.
(43) Pajerski, W.; Ochonska, D.; Brzychczy-Wloch, M.; Indyka, P.; Jarosz, M.; Golda-Cepa, M.; Sojka, Z.; Kotarba, A. Attachment Efficiency of Gold Nanoparticles by Gram-Positive and Gram-Negative Bacterial Strains Governed by Surface Charges. *J. Nanoparticle Res.* **2019**, *21* (8), 186.
(44) Halder, S.; Yadav, K. K.; Sarkar, R.; Mukherjee, S.; Saha, P.; Haldar, S.; Karmakar, S.; Sen, T. Alteration of Zeta Potential and Membrane Permeability in Bacteria: A Study with Cationic Agents. *Springerplus* **2015**, *4* (1), 1−14.
(45) Zhou, H. Y.; Zhang, Y. P.; Zhang, W. F.; Chen, X. G. Biocompatibility and Characteristics of Injectable Chitosan-Based Thermosensitive Hydrogel for Drug Delivery. *Carbohydr. Polym.* **2011**, *83* (4), 1643−1651.
(46) Chen, H.; Jin, Y.; Wang, J.; Wang, Y.; Jiang, W.; Dai, H.; Pang, S.; Lei, L.; Ji, J.; Wang, B. Design of Smart Targeted and Responsive Drug Delivery Systems with Enhanced Antibacterial Properties. *Nanoscale* **2018**, *10* (45), 20946−20962.
(47) Wu, C.; Jim, T. F.; Gan, Z.; Zhao, Y.; Wang, S. *A Heterogeneous Catalytic Kinetics for Enzymatic Biodegradation of Poly (e -Caprolactone) Nanoparticles in Aqueous Solution.* **2000**, *41*, 3593−3597.
(48) Laracuente, M. L.; Yu, M. H.; McHugh, K. J. Zero-Order Drug Delivery: State of the Art and Future Prospects. *J. Controlled Release* **2020**, *327*, 834−856.
(49) Clinical and Laboratory Standards Institute (CLSI). Performance Standards for Antimicrobial Susceptibility Testing; *Twenty-Second Informational Supplement (M100-S22)*;CLSI: Wayne, PA, 2012.
(50) Tato, M.; López, Y.; Morosini, M. I.; Moreno-Bofarull, A.; Garcia-Alonso, F.; Gargallo-Viola, D.; Vila, J.; Cantón, R. Characterization of Variables That May Influence Ozenoxacin in Susceptibility Testing, Including MIC and MBC Values. *Diagn. Microbiol. Infect. Dis.* **2014**, *78* (3), 263−267.
(51) Buchon, N.; Silverman, N.; Cherry, S. Immunity in Drosophila Melanogaster-from Microbial Recognition to Whole-Organism Physiology. *Nat. Rev. Immunol.* **2014**, *14* (12), 796−810.
(52) Nainu, F.; Djide, M. N.; Subehan, S.; Sartini, S.; Roska, T. P.; Salim, E.; Kuraishi, T. Protective Signatures of Roselle (Hibiscus Sabdariffa l.) Calyx Fractions against Staphylococcus Aureus in Drosophila Infection Model. *HAYATI J. Biosci.* **2020**, *27* (4), 306−313.
(53) Chamy, L. El; Leclerc, V.; Caldelari, I.; Reichhart, J. M. Sensing of "danger Signals" and Pathogen-Associated Molecular Patterns Defines Binary Signaling Pathways "Upstream" of Toll. *Nat. Immunol.* **2008**, *9* (10), 1165−1170.
(54) Buchon, N.; Poidevin, M.; Kwon, H.-M.; Guillou, A.; Sottas, V.; Lee, B.-L.; Lemaitre, B. A Single Modular Serine Protease Integrates Signals from Pattern-Recognition Receptors Upstream of the Drosophila Toll Pathway. *Proc. Natl. Acad. Sci. U. S. A.* **2009**, *106* (30), 12442−12447.
(55) Larrañeta, E.; Moore, J.; Vicente-Pérez, E. M.; González-Vázquez, P.; Lutton, R.; Woolfson, A. D.; Donnelly, R. F. A Proposed Model Membrane and Test Method for Microneedle Insertion Studies. *Int. J. Pharm.* **2014**, *472* (1−2), 65−73.
(56) Pamornpathomkul, B.; Ngawhirunpat, T.; Tekko, I. A.; Vora, L.; McCarthy, H. O.; Donnelly, R. F. Dissolving Polymeric Microneedle Arrays for Enhanced Site-Specific Acyclovir Delivery. *Eur. J. Pharm. Sci.* **2018**, *121* (April), 200−209.
(57) Permana, A. D.; Mir, M.; Utomo, E.; Donnelly, R. F. Bacterially Sensitive Nanoparticle-Based Dissolving Microneedles of Doxycycline for Enhanced Treatment of Bacterial Biofilm Skin Infection: A Proof of Concept Study. *International Journal of Pharmaceutics: X.* **2020**, *2*, 100047.
(58) Mir, M.; Ahmed, N.; Permana, A. D.; Rodgers, A. M.; Donnelly, R. F.; Rehman, A. U. Enhancement in Site-Specific Delivery of Carvacrol against Methicillin Resistant Staphylococcus Aureus Induced Skin Infections Using Enzyme Responsive Nanoparticles: A Proof of Concept Study. *Pharmaceutics.* **2019**, *11*, 606.


https://doi.org/10.1021/acsami.2c16857
*ACS Appl. Mater. Interfaces* XXXX, XXX, XXX−XXX